ABSTRACT

BOBOLEA, NICOLAE ALIN. Thermal Design of Wide Beam Area X-Ray Sources. (Under the direction of Dr. J. Michael Doster.)

Diffraction Enhanced Imaging (DEI) with x-ray radiation provided by a synchrotron source has been shown to provide good image contrast at lower radiation dose for materials with small x-ray attenuation coefficient As a result, DEI has received significant interest for digital mammography and other medical imaging applications. However, deployment of a synchrotron source at a medical facility is not currently feasible due to its size and costs. Consequently, a compact x-ray source capable of delivering x-ray intensities and beam collimation similar to a synchrotron accelerator is desirable.

A wide beam area x-ray source has been suggested as a possible alternative to a synchrotron source, with the x-rays generated by electron bombardment of a suitable target material. Previous research work demonstrated a prototype scale cylindrical shaped oxygen free copper target with a layer of molybdenum to be feasible from an engineering perspective. An industrial size DEI facility requires a scale-up of the proof-of-principle design. The x-ray flux necessary for high image quality implies significant heat loading on the x-ray source. Safe operation of a full scale DEI facility is reliant upon a thermal management solution capable of rejecting this heat. An active target cooling system has been proposed and its performance has been evaluated through CFD simulation. The design ensures the maximum target temperature is maintained at reasonable levels and coolant boiling is not reached under the most demanding operating conditions.

Thermal Design of Wide Beam Area X-Ray Sources

by
Nicolae Alin Bobolea

A thesis submitted to the Graduate Faculty of
North Carolina State University
in partial fulfillment of the
requirements for the Degree of
Master of Science

Nuclear Engineering

Raleigh, North Carolina

2009

APPROVED BY:

_____	_____
Dr. Mohamed A. Bourham	Dr. K. Linga Murty

_____
Dr. J. Michael Doster
Chair of Advisory Committee

DEDICATION

For Ruxandra

The one who shows me the best is always ahead.

BIOGRAPHY

Nicolae Alin Bobolea was born in 1977 in Ramnicu Valcea, Romania. Growing up in Cernavoda, near the construction site of the first nuclear power plant in Romania, he was exposed from an early age to nuclear technology as both his parents worked on the original project team. He attended Power Engineering College, POLITEHNICA University of Bucharest where he graduated with a degree in Nuclear Power Engineering in 2000 and earned his Master Degree in Nuclear Safety and Radiation Protection in the same department one year later. Working until 2002 as Teaching/Research Assistant at POLITEHNICA University, he focused on in-depth study of thermal-hydraulic modeling and simulation of nuclear systems and components. To gain experience in the nuclear industry, he spent the next five years in the Reactor Physics and Safety Analysis Department as Safety Analysis Engineer at Cernavoda Nuclear Power Plant Unit 1. The quest for professional excellence through continuous education has provided him the motivation to pursue a Master in Nuclear Engineering at North Carolina State University, starting August 2007. He worked with Dr. J. Michael Doster on thermal management of wide beam area X-ray sources, an exciting research endeavor which exposed him to new concepts and provided opportunities to learn more about innovative simulation approaches to heat transport and fluid flow using Computational Fluid Dynamics. Following graduation, he will join Reactor Operation and Accident Analysis Group at AREVA NP in Lynchburg.

ACKNOWLEDGMENTS

The author would like to thank his adviser Dr. J. Michael Doster for his valuable advice and constant support through a journey of discovery which has proven to be enriching, captivating and fruitful. It was the first opportunity to be involved in a research project that employed CFD simulations, an area he was eager to gain practical experience in for a long time. The author would also like to express his gratitude to Dr. Mohamed A. Bourham for his kind and sincere guidance as well as for his commitment to superior education through diversity and openness. Special thanks to Dr. K. Linga Murty for his help in grasping interesting and useful concepts about material science in nuclear engineering. Nevertheless, this endeavor would have never started and would not have resulted in such a rewarding accomplishment without the love, support and understanding the author constantly received from his wife Ruxandra, which was appreciated even more as she was a Nuclear Engineering graduate student at the same time.

TABLE OF CONTENTS

LIST OF TABLES

LIST OF FIGURES

LIST OF SYMBOLS

This section provides a list of symbols used throughout this thesis together with their meaning and dimensions.

Symbol	Description	Dimensions	Value
$C_{\varepsilon 1}$	k-ε turbulence model constant		1.44
$C_{\varepsilon 2}$	k-ε turbulence model constant		1.92
C_{μ}	k-ε turbulence model constant		0.09
c_p	specific heat capacity at constant volume	$m^2 \cdot s^{-2} \cdot K^{-1}$	
g	gravity vector	$m \cdot s^{-2}$	
h	specific static (thermodynamic) enthalpy	$m^2 \cdot s^{-2}$	
h_{tot}	specific total enthalpy	$m^2 \cdot s^{-2}$	
k	turbulent kinetic energy per unit mass	$m^2 \cdot s^{-2}$	
P_k	shear production of turbulence	$kg \cdot m^{-1} \cdot s^{-3}$	
p, p_{stat}	static (thermodynamic) pressure	$kg \cdot m^{-1} \cdot s^{-2}$	
p'	modified pressure	$kg \cdot m^{-1} \cdot s^{-2}$	
S_E	energy source	$kg \cdot m^{-1} \cdot s^{-3}$	
S_M	momentum source	$kg \cdot m^{-2} \cdot s^{-2}$	
T	static (thermodynamic) temperature	K	
U	vector of velocity $U_{x,y,z}$	$m \cdot s^{-1}$	
u	fluctuating velocity component in turbulent flow	$m \cdot s^{-1}$	
β	coefficient of thermal expansion (for the Boussinesq buoyancy model)	K^{-1}	
ε	turbulence dissipation rate	$m^2 \cdot s^{-3}$	

Symbol	Description	Dimensions	Value
λ	thermal conductivity	$kg \cdot m \cdot s^{-3} \cdot K^{-1}$	
μ	molecular (dynamic) viscosity	$kg \cdot m^{-1} \cdot s^{-1}$	
μ_t	turbulent viscosity	$kg \cdot m^{-1} \cdot s^{-1}$	
μ_{eff}	effective viscosity, $\mu + \mu_t$	$kg \cdot m^{-1} \cdot s^{-1}$	
ρ	density	$kg \cdot m^{-3}$	
σ_k	turbulence model constant for the k equation		1.0
σ_ε	k-ε turbulence model constant		1.3
τ	shear stress	$kg \cdot m^{-1} \cdot s^{-2}$	
ϕ	general scalar variable		

LIST OF MATHEMATICAL NOTATIONS

This section describes the basic notations that are encountered throughout this thesis.

The vector operators

Assume a Cartesian coordinate system in which i, j, k are unit vectors in the three coordinate directions. ∇ is defined as:

$$\nabla = \left[\frac{\partial}{\partial x}, \frac{\partial}{\partial y}, \frac{\partial}{\partial z} \right]$$

The gradient operator

For a general scalar function $\phi(x, y, z)$, the gradient of ϕ is defined by:

$$\nabla\phi = \frac{\partial\phi}{\partial x} i + \frac{\partial\phi}{\partial y} j + \frac{\partial\phi}{\partial z} k$$

Divergence operator

For a vector function $U(x, y, z)$ where:

$$U = \begin{bmatrix} U_x \\ U_y \\ U_z \end{bmatrix}$$

the divergence of U is defined by:

$$\nabla \bullet U = \frac{\partial U_x}{\partial x} + \frac{\partial U_y}{\partial y} + \frac{\partial U_z}{\partial z}$$

Dyadic operator

The dyadic operator (or tensor product) of two vectors, U and V, is defined as:

$$U \otimes V = \begin{bmatrix} U_x V_x & U_x V_y & U_x V_z \\ U_y V_x & U_y V_y & U_y V_z \\ U_z V_x & U_z V_y & U_z V_z \end{bmatrix}$$

In specific tensor notation, the following expression can be written:

$$\nabla \bullet (\rho U \otimes U) = \begin{bmatrix} \frac{\partial}{\partial x}(\rho U_x U_x) + \frac{\partial}{\partial y}(\rho U_y U_x) + \frac{\partial}{\partial z}(\rho U_z U_x) \\ \frac{\partial}{\partial x}(\rho U_x U_y) + \frac{\partial}{\partial y}(\rho U_y U_y) + \frac{\partial}{\partial z}(\rho U_z U_y) \\ \frac{\partial}{\partial x}(\rho U_x U_z) + \frac{\partial}{\partial y}(\rho U_y U_z) + \frac{\partial}{\partial z}(\rho U_z U_z) \end{bmatrix}$$

Matrix transposition

The transpose of a matrix is defined by the operator T. The following example is provided for illustration.

$$\nabla \phi = \begin{bmatrix} \frac{\partial \phi}{\partial x} \\ \frac{\partial \phi}{\partial y} \\ \frac{\partial \phi}{\partial z} \end{bmatrix} \quad \rightarrow \quad [\nabla \phi]^T = \begin{bmatrix} \frac{\partial \phi}{\partial x} & \frac{\partial \phi}{\partial y} & \frac{\partial \phi}{\partial z} \end{bmatrix}$$

The Identity Matrix (Kronecker Delta function)

The Identity matrix is defined by:

$$\delta = \begin{bmatrix} 1 & 0 & 0 \\ 0 & 1 & 0 \\ 0 & 0 & 1 \end{bmatrix}$$

Chapter 1 Introduction

1.1 Wide Beam Area X-ray Sources

Diffraction Enhanced Imaging (DEI) is an investigation method which provides good contrast at lower radiation dose for materials with small x-ray attenuation coefficient. Historically, DEI images have been produced with x-ray radiation provided by a synchrotron source. The typical DEI set-up includes a monochromator which selects a very narrow x-ray energy band, strongly collimates the monochromatized beam and directs it towards the object. The exiting beam from the object passes through a crystal analyzer and is diffracted onto the detector producing higher quality images than conventional imaging devices. Although DEI has potential medical applications, one of the most suitable being mammography, deployment of a synchrotron source at a medical facility is not feasible due to size and cost of the synchrotron installation.

A wide beam area x-ray source has been suggested as a possible alternative to a synchrotron source, where the x-rays are produced by electron bombardment of an appropriate target material. The x-ray source should provide an x-ray flux comparable to the synchrotron source flux, appropriate x-ray energy range for mammography and a large field of view. Previous investigations based on a cylindrical shaped oxygen free copper target with a layer of molybdenum have shown the approach to be viable [9], [10].

To satisfy the requirements of an industrial scale system, a scale-up of the proof-of-principle design is necessary. Since most of the electron beam energy is absorbed as heat in the target, a thermal management solution that addresses this concern for an industrial scale device was developed. This research work embodies the design and computational simulations of an active cooling system which provides adequate target heat rejection capabilities.

1.2 Simulation using Computational Fluid Dynamics

Computational Fluid Dynamics (CFD) is a computer based tool for simulating the behavior of systems involving fluid flow, heat transfer and other physical processes. This is accomplished by solving the equations of fluid flow (in a special form) over a region of interest, with specified (known) conditions on the boundary of that region. Historically, the foundation of experimental fluid dynamics was laid in France and England in the seventeenth century and it is seen as “the first approach” to development of this discipline, [1]. For the following two centuries, in parallel with the advances in experimental research, “a second approach” to fluid dynamics has gradually made its presence felt, namely theoretical fluid dynamics. Until the dawn of the high speed digital computing era, the study and practice of fluid dynamics was dominated by either pure experiment or pure theory. Rapid increases in computing power coupled with the development of accurate numerical algorithms have produced a fundamentally new approach in fluid dynamics – Computational Fluid Dynamics.

Although computers have been used to solve fluid flow problems for many years, recent advances in computing power, together with powerful graphics and interactive 3D manipulation of models have made the process of creating a CFD model and analyzing results much less labor intensive, reducing time and cost. Consequently, Computational Fluid Dynamics is now an established industrial and research tool, helping to reduce design time and improve process efficiency. CFD provides a cost-effective and accurate alternative to scale model testing, with variations on the simulation being performed quickly, offering obvious advantages.

CFD can be used to determine the performance of a component at the design stage. This enables the designer to improve and optimize the design relative to specific design criteria. The process of performing a CFD simulation can be split into four components, [2]:

1. Creating the geometry/mesh,
2. Defining the physics of the CFD model,
3. Solving the CFD problem,
4. Post-processing and visualizing the results.

The creation of the geometry/mesh is the first interactive process in the pre-processing stage. The objective is to produce a high quality mesh that provides a good approximation of the design geometry. Before a mesh can be produced, a close geometric solid is required. For this study, the geometry is created using Autodesk Inventor Professional 2008, a powerful 3D CAD package that allows rapid 3D solid model development.

Additionally, Autodesk Inventor has the capability of exporting the geometry file in a suitable format for the meshing process. The meshing tool used in this study is ANSYS ICEM CFD 11.0. ICEM CFD is a versatile tool that allows mesh creation for complicated solids and has proven to be easy to learn, straightforward to use and relatively forgiving with inexperienced users.

Defining the physics of the model is an interactive process in the second pre-processing stage and its main purpose is to create the input required by the CFD solver. Based on the mesh files loaded into the physics pre-processor, solid and fluid domains of interest are created and physical models are attached to the domains as required for solution of the problem. Also, fluid properties, boundary conditions and material properties have to be specified before the model is complete. The software used in this study for the second pre-processing stage is ANSYS CFX-Pre which ensures a simple CFD model development.

The solution to the CFD problem is obtained by running the CFD solver based on the complete definition of the physical model. A CFD problem is solved as follows:

1. The partial differential equations that describe the phenomena of interest (mainly Navier-Stokes equations and equations derived from the turbulence models) are integrated over all volumes in the region of interest. This is equivalent to applying the basic conservation laws to each control volume.
2. These integral equations are converted to a system of algebraic equations by generating a set of approximations for the terms in the integral equations.
3. The algebraic equations are solved iteratively.

An iterative approach is required because of the non-linear nature of the equations, and, as the solution approaches the exact solution, it is said to converge. For each iteration, an error or residual is determined as a measure of the overall conservation of the flow properties. The proximity of the final solution to the exact solution is a function of a number of factors among which the size and shape of the control volumes as well as the size of the final residuals are the most important. Besides these, modeling of complex physical processes such as turbulence relies on empirical relationships. Consequently, the approximations inherent in these models also contribute to the differences between the CFD solution and the real flow. Once the ANSYS CFX-Solver has computed a solution for the problem, it prepares a file containing the variables of interest and their final solution values in selected locations of the analyzed domain.

Visualizing the result in the post-processor is the last step of a CFD simulation. Post-processing allows interactive inspection of the results and includes a wide array of options, from obtaining point values to generation of complex animated sequences. The post-processing capabilities offered by ANSYS CFX-Post used in this study are visualization of geometry and control volumes, vector plots showing the direction and the magnitude of the flow, and visualization of the variation of scalar variables (variables which have only magnitude, not direction, such as temperature and pressure) throughout the domain of interest.

The approach described here provides the basis for the simulation work to determine a viable design for adequate cooling of wide beam area x-ray sources. Several preliminary designs are evaluated that eventually lead to the final solution presented in detail later.

Chapter 2 Theory

This chapter provides a brief review of CFD, [3], [4]. The set of equations which describe the motion of viscous, non-compressible fluids are known as the Navier-Stokes equations. These partial differential equations were derived independently in the early nineteenth century by the French engineer and physicist Claude-Louise Navier and English mathematician and physicist George Gabriel Stokes. The equations have no general analytical solution but can be discretized and solved numerically. Equations describing other processes can be solved in conjunction with Navier-Stokes equations. These equations can be derived from approximating models, turbulence models constituting an excellent example.

There are a number of different numerical solution methods which are currently used in CFD codes. One of the most common is the finite volume technique. In this technique, the region of interest – a domain – is divided into small three dimensional pieces – usually tetrahedrons – called control volumes. The equations for the process of interest in the small sub-region are discretized and solved iteratively. As a result, an approximate value for each variable is obtained at specific points through the domain. Using post-processing and visualization tools, a complete picture of the model behavior can be assembled.

2.1 Basic Governing Equations

ANSYS CFX solves the unsteady Navier-Stokes equations in their conservative form [3]. The instantaneous conservation equations of mass, momentum and energy are averaged producing additional terms that account for turbulent flows. The instantaneous equation of mass – the continuity equation – can be written as:

$$\frac{\partial \rho}{\partial t} + \nabla \bullet (\rho U) = 0 \tag{2.1}$$

The momentum equation can be expressed as:

$$\frac{\partial (\rho U)}{\partial t} + \nabla \bullet (\rho U \otimes U) = -\nabla p + \nabla \bullet \tau + S_M \tag{2.2}$$

The stress tensor τ, is related to the strain rate by:

$$\tau = \mu \left(\nabla U + (\nabla U)^T - \frac{2}{3} \delta \nabla \bullet U \right) \tag{2.3}$$

The total energy equation is:

$$\frac{\partial (\rho h_{tot})}{\partial t} - \frac{\partial p}{\partial t} + \nabla \bullet (\rho U h_{tot}) = \nabla \bullet (\lambda \nabla T) + \nabla \bullet (U \bullet \tau) + U \bullet S_M + S_E \tag{2.4}$$

Where h_{tot} is the total enthalpy, related to the static enthalpy $h(T, p)$, by:

$$h_{tot} = h + \frac{1}{2} U^2 \tag{2.5}$$

The static enthalpy (the measure of the energy contained in a fluid per unit mass) is given by:

$$h = u_{stat} + \frac{p_{stat}}{\rho_{stat}} \tag{2.6}$$

The viscous work term $\nabla \bullet (U \bullet \tau)$ represents the work due to viscous stresses.

The term $U \bullet S_M$ represents the work due to external momentum sources and in the current implementation of ANSYS CFX-Solver is neglected.

In addition to the fluid conservation equations, a thermodynamic equation of state is required for the fluid of interest.

Since simulation work for this thesis involves both fluid and solid domains, it is important to mention the available options for simulation of heat transfer. This is known as conjugate heat transfer and uses a simplified conservation of the energy equation which takes into consideration only the conduction mode of heat transfer:

$$\frac{\partial}{\partial t}(\rho c_p T) = \nabla \bullet (\lambda \nabla T) + S_E \qquad (2.7)$$

In Eq. (2.7), ρ, c_p and λ are the density, specific heat capacity and thermal conductivity of the solid, respectively.

It is important to make a special note regarding variable values at the solid-fluid interface. The solution to a CFD problem, as calculated by ANSYS CFD-Solver, uses finite volume elements, which are not the same as the mesh elements. Each node in the mesh is at the center of a finite volume element. As a result, the value of some variables at the boundary nodes (i.e., on the edges of the geometry) are not precisely equal to the specified boundary conditions (e.g., velocity near the wall will not be exactly zero).

For visualization purposes, it is recommended to use the hybrid variable values. The hybrid variable value on a solid-fluid interface is single valued and takes the solid side conservative value.

For a temperature profile, between the interface and the first node in the fluid an interpolated value is calculated from the solid-side interface value and the first fluid node value. No discontinuity in the temperature profile will be seen across the solid-fluid interface.

For quantitative calculations, a different approach is recommended. This approach makes use of conservative variable values. The conservative value for the solid-side node of a solid-fluid interface is obtained by averaging the value of the variable over the half of the control volume that lies inside the solid. Accordingly, the conservative value for the fluid-side node of a solid-fluid interface is determined by averaging the variable value over the half of the control volume that lies inside the fluid. For the case of heat transfer from a hot solid to a cool fluid, a temperature plot across the solid-fluid interface will reveal a sharp change in temperature and a temperature discontinuity will be visible at the interface. It should be noted that the results reported in this study use only conservative values.

2.2 Boundary Conditions

As mentioned previously, the solution to a CFD problem requires boundary conditions (BC). Detailed treatment of boundary condition mathematics can be found in Ref. [5]. The types of boundary conditions used in the development of thermal design models for

wide beam area x-ray sources are inlet, outlet and wall. Their implementation is consistent with Ref. [2]. Each BC type will be briefly discussed further.

Inlet – For the inlet boundary condition, the normal speed in option has been selected because it provides better simulation stability and convergence and it is a convenient way of specify one of the main parameters of the design. The direction of the velocity is normal to the boundary and constraints are imposed such that the flow direction is parallel to the boundary surface normal, for each element face at the boundary. As far as heat transfer is concerned, a constant inlet temperature is specified for this type of boundary condition.

Outlet – The outlet boundary condition utilizes an outlet relative static pressure which is constrained such that its average value equals the value specified as input. The constraint is imposed by the use of Eq. (2.8).

$$\bar{p}_{spec} = \frac{1}{A}\int_S p_n \, dA \qquad (2.8)$$

The integral in Eq. (2.8) is over the entire outlet boundary surface and p_n is the pressure of node n on the boundary surface.

Wall – This type of boundary condition is used define the physical limits for domain of interest that is investigated. When the domain under scrutiny is a fluid domain, the velocity of the fluid at the wall boundary is set to zero. However, for a solid domain a heat flux at the wall boundary has to be specified. The heat flux can be entered either as a constant value or as a variable that stores a three dimensional flux distribution.

2.3 Turbulence Model

The turbulence model selected for the simulation of this design is the k-epsilon model, [6], [7], [8]. It is an industry standard model which has proven to be stable and numerically robust while at the same time offering good solution accuracy. Model implementation in ANSYS CFX benefits from the scalable wall-function approach which enables a CFD solution to be achieved on arbitrary near wall grids when the mesh is fine with positive impact on precision of flow prediction. This section will describe shortly the mathematics behind the k-epsilon model using the approach from Ref. [3].

Although, the Navier-Stokes equations are capable of describing both laminar and turbulent flows without need for additional information, turbulent flows at realistic Reynolds numbers would generally require length scales much smaller than the smallest practical finite volume mesh. On the other hand Direct Numerical Simulation (DNS) of these types of flows requires computing power way beyond the capabilities available today or in the foreseeable future. Consequently, statistical turbulence models have been developed which modify the original unsteady Navier-Stokes equations by considering that turbulent flows exhibit, at time scales much larger than the time scales of turbulent fluctuations, average characteristics with an additional time-varying component. This assumption leads to the development of Reynolds Averaged Navier-Stokes (RANS) equations which greatly reduces the computational effort compared to the Direct Numerical Simulations, but also introduces additional unknown terms containing products of the fluctuating quantities, which act as additional stresses in the fluid.

These “turbulent” or “Reynolds” stresses are difficult to determine directly and become further unknowns. In order to have sufficient number of equations for all unknowns, the Reynolds stresses needs to be modeled by additional equations of known quantities. The equations to close the system define the turbulence model.

As hypothesized, the velocity may be divided into an average component, $\overline{U}$, and a time varying component, u.

$$U = \overline{U} + u \tag{2.9}$$

The average component is given by:

$$\overline{U} = \frac{1}{\Delta t}\int_{t}^{t+\Delta t} U dt \tag{2.10}$$

where Δt is a time scale that is large relative to the turbulent fluctuations, but small relative to the time scale to which the equations are solved.

The Reynolds-averaged equations are obtained by introducing the averaged quantities into the original transport equations. In the equations below, the bar is dropped for averaged quantities, except for products of fluctuation quantities.

$$\frac{\partial \rho}{\partial t} + \nabla \bullet \left(\rho U\right) = 0 \tag{2.11}$$

$$\frac{\partial \rho U}{\partial t} + \nabla \bullet \left\{\rho U \otimes U\right\} = \nabla \bullet \left\{\tau - \rho\overline{u \otimes u}\right\} + S_M \tag{2.12}$$

where τ is the molecular stress tensor.

As it can be seen, the continuity equation has not changed but the momentum equation contains a turbulent flux term, $\rho\overline{u \otimes u}$, known as the Reynolds stress, in addition to the molecular diffusive fluxes. This term reflects that the convective transport due to turbulent velocity fluctuations will increase mixing over and above that caused by thermal fluctuations. For high Reynolds numbers, the length scale of turbulent velocity fluctuations is much larger than the mean free path of the thermal fluctuations at the molecular level, so turbulent fluxes are much larger than molecular fluxes.

The Reynolds-averaged energy equation is:

$$\frac{\partial \rho h_{tot}}{\partial t} - \frac{\partial p}{\partial t} + \nabla \bullet \left(\rho U h_{tot}\right) = \nabla \bullet \left(\lambda \nabla \tau - \rho \overline{uh}\right) + \nabla \bullet \left(U \bullet \tau\right) + S_E \qquad (2.13)$$

An additional turbulence flux term appears in Eq. (2.13) compared with Eq. (2.4). As previously mentioned, the $\nabla \bullet \left(U \bullet \tau\right)$ term is the viscous work term.

The total enthalpy, h_{tot}, is given by:

$$h_{tot} = h + \frac{1}{2}U^2 + k \qquad (2.14)$$

It is worth noting that in Eq. (2.14), the total enthalpy contains the turbulent kinetic energy, k, which is given by:

$$k = \frac{1}{2}\overline{u^2} \qquad (2.15)$$

One of the treatments adopted for turbulence models that allows the closure of Reynolds-averaged equations are the eddy viscosity models. It has been suggested that turbulence consists of small eddies which are continuously forming and dissipating and the

Reynolds stresses are assumed to be proportional to the mean velocity gradients. The implementation of eddy viscosity models used throughout this thesis for CFD simulations is based on the two equation k-epsilon model.

In the k-epsilon model, k is the turbulence kinetic energy, defined as the variance of the fluctuations in the velocity, and has dimensions of m^2/s^2. ε is the turbulence eddy dissipation (the rate at which the velocity fluctuations dissipate), and has dimensions of k per unit time, m^2/s^3. Because the k-ε model introduces two new variables, a revised system of equations will be presented further. The continuity equation is:

$$\frac{\partial \rho}{\partial t} + \nabla \bullet (\rho U) = 0 \tag{2.16}$$

The new momentum equation can be written as:

$$\frac{\partial \rho U}{\partial t} + \nabla \bullet (\rho U \otimes U) - \nabla \bullet (\mu_{eff} \nabla U) = -\nabla p' + \nabla \bullet (\mu_{eff} \nabla U)^T + B \tag{2.17}$$

where B is the sum of the body forces, μ_{eff} is the effective viscosity accounting for turbulence and p' is the modified pressure. The modified pressure is defined as:

$$p' = p + \frac{2}{3}\rho k + \frac{2}{3}\mu_t \nabla \bullet U \tag{2.18}$$

For the purpose of this study it has been assumed that $p' = p$, as it is implemented as default setting in the ANSYS CFX-Solver.

The effective viscosity is expressed as:

$$\mu_{eff} = \mu + \mu_t \tag{2.19}$$

where μ_t is the turbulence viscosity.

The k-ε model is based on the assumption that there is a relation between the turbulence viscosity and the turbulence kinetic energy and turbulence dissipation rate. This relation is:

$$\mu_t = C_\mu \rho \frac{k^2}{\varepsilon} \tag{2.20}$$

where C_μ is a constant.

The values for k and ε come from the differential transport equations for the turbulence kinetic energy and turbulence dissipation rate:

$$\frac{\partial(\rho k)}{\partial t} + \nabla \bullet (\rho U k) = \nabla \bullet \left[\left(\mu + \frac{\mu_t}{\sigma_k} \right) \nabla k \right] + P_k - \rho\varepsilon \tag{2.21}$$

$$\frac{\partial(\rho \varepsilon)}{\partial t} + \nabla \bullet (\rho U \varepsilon) = \nabla \bullet \left[\left(\mu + \frac{\mu_t}{\sigma_\varepsilon} \right) \nabla \varepsilon \right] + \frac{\varepsilon}{k} (C_{\varepsilon 1} P_k - C_{\varepsilon 2} \rho \varepsilon) \tag{2.22}$$

where $C_{\varepsilon 1}, C_{\varepsilon 2,}$ σ_k and σ_ε are constants.

P_k is the turbulence production due to viscous and buoyancy forces, which is modeled using:

$$P_k = \mu_t \nabla U \bullet \left(\nabla U + \nabla U^T \right) - \frac{2}{3} \nabla \bullet U (3\mu_t \nabla \bullet U + \rho k) + P_{kb} \tag{2.23}$$

It should be mentioned that for incompressible flow, the term $\nabla \bullet U$ is small and the contribution to the production of $\frac{2}{3} \nabla \bullet U (3\mu_t \nabla \bullet U + \rho k)$ term is of less significance.

The P_{kb} term from Eq. (2.23) is the buoyancy production and it can be modeled in two ways. For the full buoyancy model, P_{kb} is represented by:

$$P_{kb} = -\frac{\mu_t}{\rho\sigma_p} g \bullet \nabla\rho \tag{2.24}$$

If the Boussinesq buoyancy model is considered, the following equation is used:

$$P_{kb} = \frac{\mu_t}{\rho\sigma_p} \rho\beta_g \bullet \nabla T \tag{2.25}$$

The buoyancy production term is included in the k equation if the buoyancy turbulence option selected in the CFD model is production. If P_{kb} is positive and the option selected is production and dissipation, the term is included in the ε equation using the following formula:

$$P_{\varepsilon b} = C_3 \cdot \max(0, P_{kb}) \tag{2.26}$$

The values for buoyancy turbulence model constants are given by:

$\sigma_p = 0.9$ for Boussinesq buoyancy, $\sigma_p = 1$ for full buoyancy model and $C_3 = 1$.

The simulations performed for this thesis use the Boussinesq buoyancy model and the buoyancy turbulence modeling uses the production and dissipation option. The motivation behind this selection is that the temperature does not change significantly throughout the fluid domain.

Chapter 3 Computational Simulation

The design requirements associated with a viable thermal management solution capable of providing sustainable operating conditions for a wide beam area x-ray source are presented in the first part of this chapter. Based on these requirements, a short review of initial target cooling system designs, which highlights different options investigated, is portrayed. Lastly, the final design solution is discussed in detail.

3.1 Design Requirements

Due to high thermal loads during operation, wide area x-ray sources require an active cooling system designed to satisfy the following requirements:

1. Maximum allowable target temperature must be significantly lower than the melting point of the target material. Uniform and non-uniform heat flux distributions are used to assess the design compliance with this criterion.

2. The target cooling design has to minimize the pumping power associated with the fluid flow. This concern is addressed by creating a geometry that provides small hydraulic resistance as well as by a judicious selection of the coolant inlet velocity.

3. Heat transfer at the solid/liquid interface is by single phase forced convection. Since the coolant is water, operating limits have to be identified and established such that no coolant boiling occurs.

3.2 Initial Designs

This section is dedicated to providing an overview of the target design evolution. Emphasis will be put on characteristic features, model simulation results and conclusions which, at each step, have shaped the progress of this research work.

3.2.1 Initial Design 01

The first option investigated as a solution for thermal management of wide beam area x-ray sources has its roots in a study of smaller scale targets, [9], [10], and assumes an impinging cooling jet on the back of the target. Based on the recommendations from [9], [10], the target area of the original prototype design has been magnified by a factor of 4.04 and the rest of the dimensions adjusted accordingly, as presented in Table 3.1. Additionally, eight circumferential evenly distributed fins have been added to the back of the target which serves the following purposes:

- to provide a uniform coolant flow distribution over the target surface,
- to enhance the heat transfer through use of heat dissipating fins.

Figure 3.1 presents the geometry of initial design 01.

Table 3.1 – Initial design 01 characteristics

Parameter	Value
Inlet diameter [mm / inch]	68.0 / 2.68
Inlet area [mm^2 / $inch^2$]	3631.68 / 5.63
Nozzle diameter [mm / inch]	28.8 / 1.13
Nozzle area [mm^2 / $inch^2$]	651.44 / 1.01
Outlet area [mm^2 / $inch^2$]	6625.65 / 10.27
Fin thickness [mm / inch]	2.0 / 0.0787
Heated target diameter [mm / inch]	132.4 / 5.213
Heated target area [mm^2 / $inch^2$]	13767.84 / 21.34
Target thickness [mm / inch]	10.8 / 0.425
Water volume [cm^3 / $inch^3$]	2457.5 / 149.97
Metal volume [cm^3 / $inch^3$]	1244.6 / 75.95

The coolant (water) enters through the central pipe, is accelerated through the jet, flows through the channels on the back of the target and returns to the exit. The target is entirely from copper and the copper thermal properties used in the simulations are those available in the ANSYS CFX library. Simulations have been performed for this design for inlet water velocity of 1, 2 and 3 m/s (3.28, 6.56 and 9.84 ft/s) and inlet water temperature of 293 °K (67.73 °F). A uniform heat flux equivalent to a power level of 180 kW was imposed. As a result, the target was subjected to a heat flux of $13.08 \cdot 10^6$ W/m^2 ($4.146 \cdot 10^6$ Btu/h·ft^2) which was modeled as a boundary condition. Since no heat transfer from the target to the

surroundings has been taken into account, the simulations provide conservative results. A summary of simulation results is presented in Table 3.2 and 3.3.

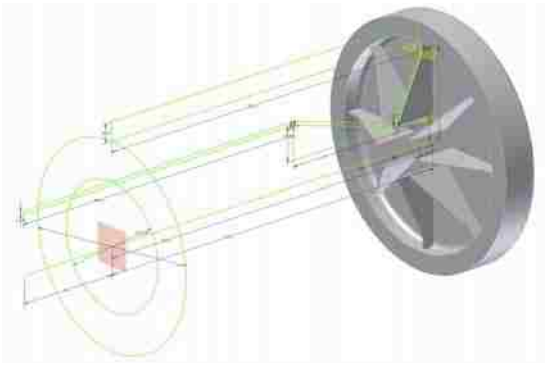

a) Fins and flow channels

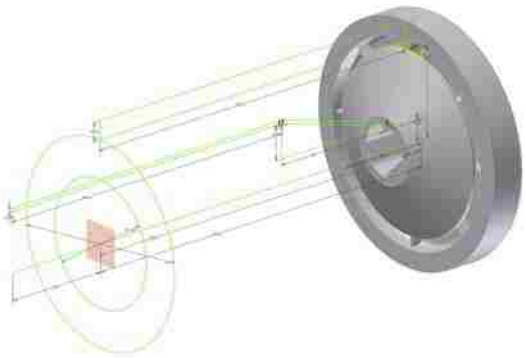

b) Jet top wall

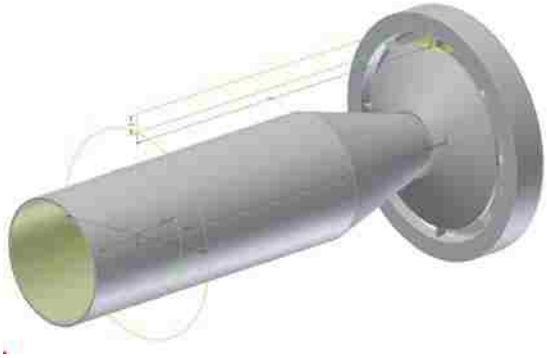

c) Inlet pipe and jet top wall

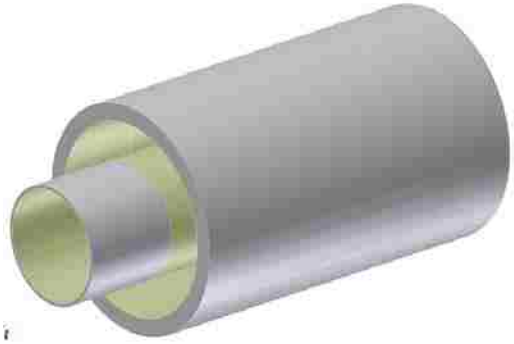

d) Complete design

Figure 3.1 – Initial design 01 geometry

Table 3.2 – Initial design 01 simulation results (SI units)

Parameter	Inlet velocity [m/s]		
	1	2	3
Maximum target temperature [°K]	1223.0	1023.95	939.84
Pumping power [W]	50.99	407.24	1372.51
Maximum water temperature [°K]	325.39	310.19	305.10
Maximum water velocity [m/s]	6.65	13.5	20.51
Coolant mass flow [kg/s]	3.62	7.23	10.85
Minimum system pressure [Pa]	91478.90	63282.3	9190.27
Maximum system pressure [Pa]	118533.0	174093.0	266595.0
Outlet static pressure [Pa]	100000.0	100000.0	100000.0

The maximum target temperature for the flow regimes analyzed is 1223.0 °K (1741.73 °F). Although this value is less than the copper melting temperature of 1356 °K (1981.13 °F), one must bear in mind that this value has been calculated taking into account a uniform heat flux distribution. Little margin is left for a non-uniform heat flux distribution which would be closer to the real operating conditions. In addition, a flow stagnation point develops in the center of the target at the location that corresponds to the maximum target temperature, as illustrated in Figure 3.2. Increasing inlet water velocity decreases target temperature, but at the same time requires more pumping power.

Table 3.3 – Initial design 01 simulation results (British units)

Parameter	Inlet velocity [ft/s]		
	3.28	6.56	9.84
Maximum target temperature [°F]	1741.73	1383.44	1232.04
Pumping power [hp]	0.0684	0.546	1.84
Maximum water temperature [°F]	126.1	98.67	89.51
Maximum water velocity [ft/s]	21.82	44.29	67.29
Coolant mass flow [lb/s]	7.981	15.94	23.92
Minimum system pressure [psi]	13.27	9.18	1.33
Maximum system pressure [psi]	17.19	25.25	38.67
Outlet static pressure [psi]	14.5	14.5	14.5

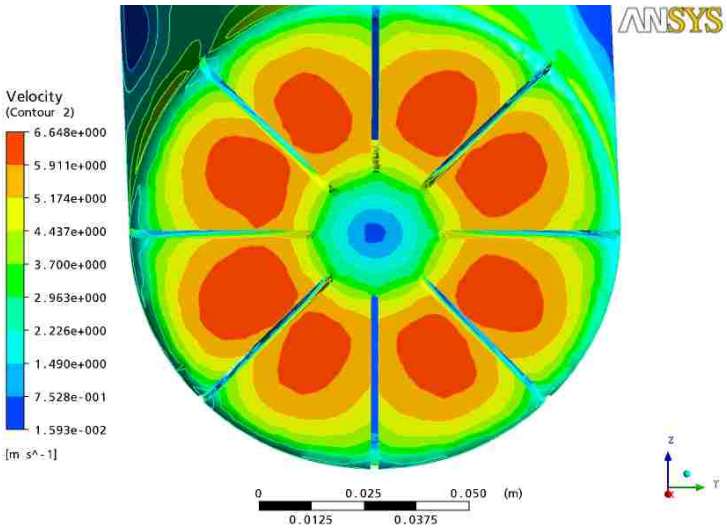

a) Flow stagnation – water target interface

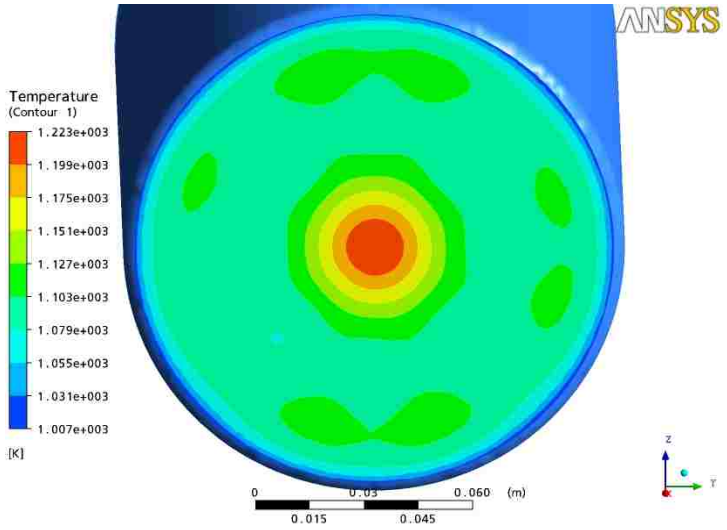

b) Target temperature distribution

Figure 3.2 – Flow stagnation and target temperature for inlet velocity 1 m/s

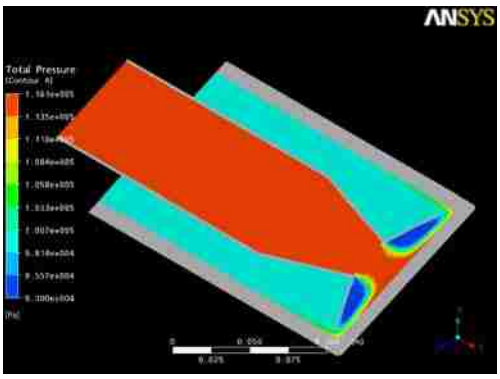

a) Pressure profile – 1 m/s

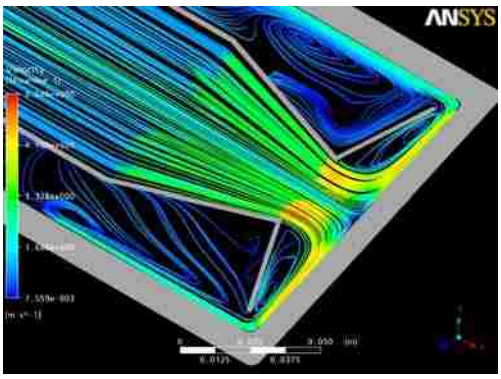

b) Velocity profile – 1 m/s

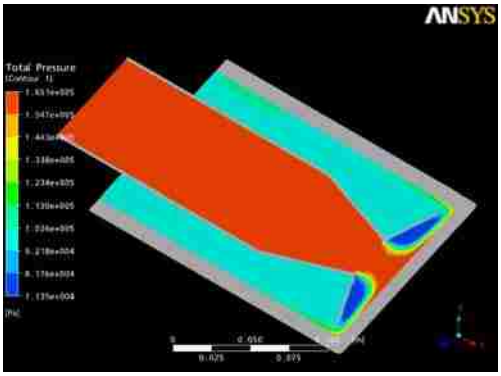

c) Pressure profile – 2 m/s

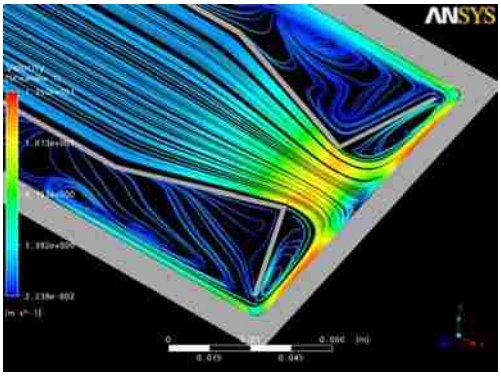

d) Velocity profile – 2 m/s

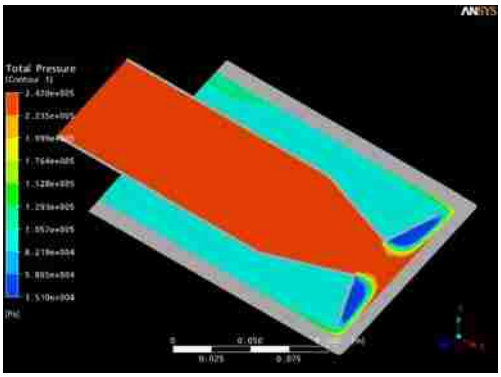

e) Pressure profile – 3 m/s

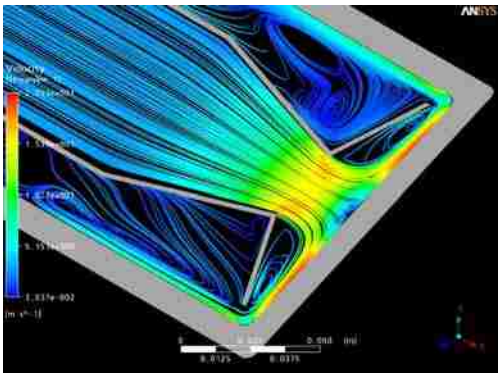

f) Velocity profile – 3 m/s

Figure 3.3 – Velocity and pressure profiles in the radial flow channels

High mass flow rates result in increased maximum water velocity which may raise additional issues related to vibrations and possible material erosion and would require further investigation. Generally, the maximum pressure of the system becomes an important factor since it is desirable to have a high flow - low pressure cooling system.

Based on Figure 3.3, an evaluation of pressure and velocity profiles in the radial flow channels of this design is presented. Although maximum target temperatures are reduced with increasing inlet velocity, there are several shortcomings that need to be highlighted. For any inlet velocity, as the water exits the jet and hits the back of the target, a vortex region develops directly under the jet top wall, as seen in Figure 3.3 – b), d) and f). In this region, a pronounced drop in pressure is observed, as shown by Figure 3.3 – a), c) and e). As the inlet water velocity increases, the pressure drop becomes more and more significant. An increase in water temperature in this region may cause localized boiling to occur.

The potential for coolant boiling, coupled with high temperatures in the center of the target as a result of flow stagnation are the main reasons this design has not been developed further. However, it was observed that maximizing the areas of high velocity flow across the heated surface may provide better heat transfer, no flow stagnation points as well as reduced pressure losses which positively impact the pumping power. This observation is the basis for development of subsequent designs.

3.2.2 Initial Design 02

The presence of a flow stagnation point in the center of the target is one of the most significant drawbacks of initial design 01. In order to mitigate this issue, a new approach has been envisioned. The main attribute of this design is to change the flow direction from a direction that is perpendicular to the back of the target to one that is parallel to the back of the target. This idea is embodied in the initial design 02.

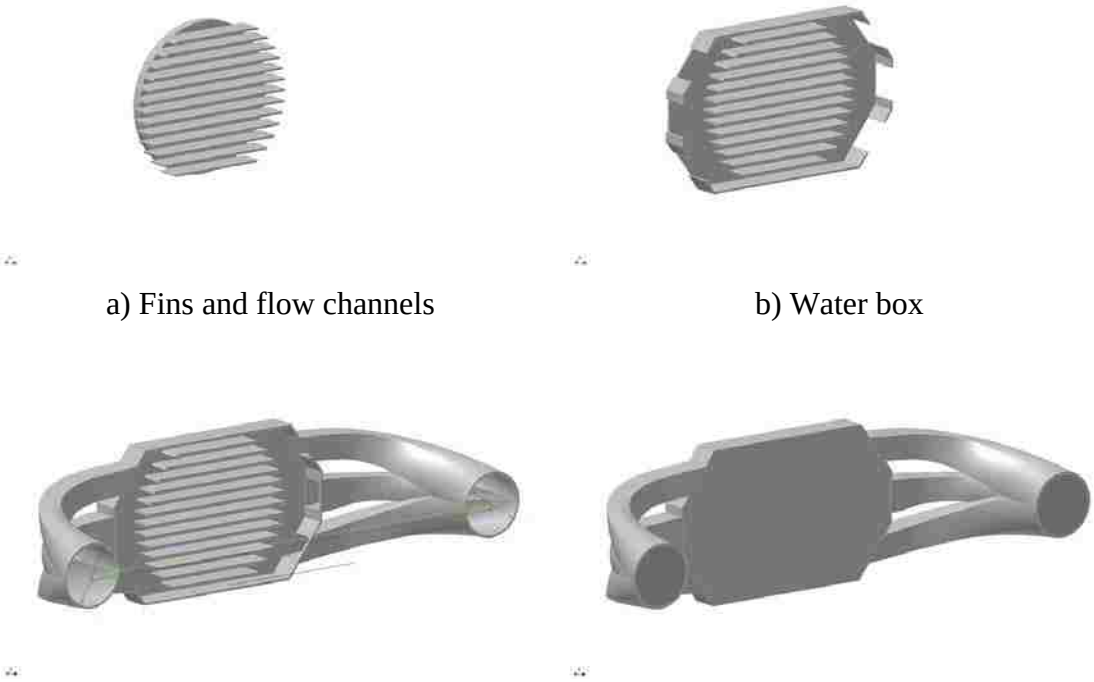

a) Fins and flow channels

b) Water box

c) Transparent back

d) Complete design

Figure 3.4 – Initial design 02 geometry

As illustrated in Figure 3.4, an array of flow channels is positioned horizontally on the back of the target. The water flows through these channels from right to left. The flow channels are enclosed in the water box. The water is supplied to the water box through three distribution channels which are connected to a common inlet header. The heated water is discharged from the water box through the three channels on the left which converge in a common outlet header. Because of the high velocity water jet that sweeps the back of the target, no obvious flow stagnation points are likely to develop.

Table 3.4 – Initial design 02 characteristics

Parameter	Value
Inlet diameter [mm / inch]	56.0 / 2.205
Inlet area [mm^2 / $inch^2$]	2463.0 / 3.82
Outlet diameter [mm / inch]	56.0 / 2.205
Outlet area [mm^2 / $inch^2$]	2463.0 / 3.82
Fin thickness [mm / inch]	2.0 / 0.0787
Fin height [mm / inch]	20.0 / 0.787
Heated target diameter [mm / inch]	132.4 / 5.213
Heated target area [mm^2 / $inch^2$]	13767.84 / 21.34
Target thickness [mm / inch]	10.8 / 0.425
Water volume [cm^3 / $inch^3$]	1109.2 / 67.69
Metal volume [cm^3 / $inch^3$]	511.12 / 31.19

The heated area of the target is the same as for initial design 01 and the simulations were performed at the same power level of 180 kW. The inlet water temperature is 293 °K (67.73 °F) and inlet coolant velocities considered in the performance analysis of this design are 3, 4 and 5 m/s (9.84, 13.12 and 16.4 ft/s).

Table 3.5 – Initial design 02 simulation results (SI units)

Parameter	Inlet velocity [m/s]		
	3	4	5
Maximum target temperature [°K]	1183.67	1105.37	1051.55
Pumping power [W]	246.69	571.78	1093.99
Maximum water temperature [°K]	395.64	380.05	372.57
Maximum water velocity [m/s]	11.61	15.58	19.58
Coolant mass flow [kg/s]	7.35	9.80	12.25
Minimum system pressure [Pa]	72300.1	50612.9	23133.2
Maximum system pressure [Pa]	151364.0	189880.0	238417.0
Outlet static pressure [Pa]	100000.0	100000.0	100000.0

The maximum target temperature is less than the melting temperature of copper. Though a closer look at the simulation results presented in Table 3.5 or Table 3.6 reveals that the maximum water temperature is very high and, combined with a low local pressure due to inadequate flow distribution in the flow channels, coolant boiling may appear.

Table 3.6 – Initial design 02 simulation results (British units)

Parameter	Inlet velocity [ft/s]		
	9.84	13.12	16.4
Maximum target temperature [°F]	1670.94	1530.0	1433.12
Pumping power [hp]	0.3308	0.7668	1.467
Maximum water temperature [°F]	252.5	224.4	211.0
Maximum water velocity [ft/s]	38.09	51.12	64.24
Coolant mass flow [lb/s]	16.2	21.61	27.01
Minimum system pressure [psi]	10.49	7.341	3.355
Maximum system pressure [psi]	21.95	27.54	34.58
Outlet static pressure [psi]	14.5	14.5	14.5

Figure 3.5.a) shows that the flow distribution through the horizontal channels is non-uniform; the high, mid and low positioned channels receive most of the flow while there are two channels in the upper half and two channels in the lower half of the target that get very low coolant flow. The reason for this resides in the position and flow areas of the inlet distribution channels. As indicated in Figure 3.5.b), the highest target temperatures occur in the four low flow channels. Consequently, the coolant reaches its highest temperature in these four channels.

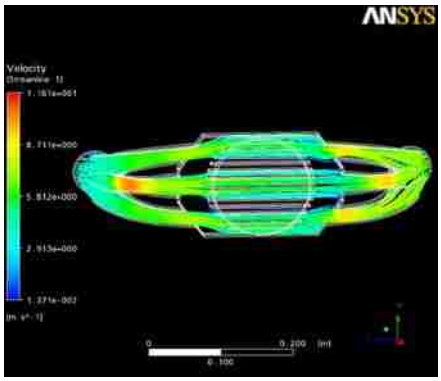

a) Velocity streamline

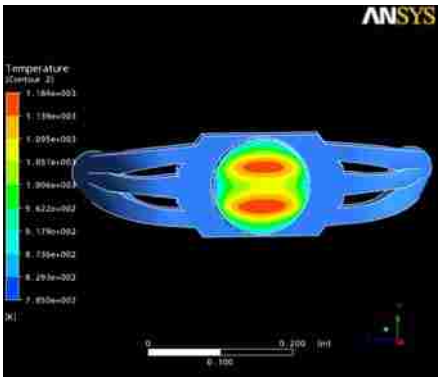

b) Target temperature profile

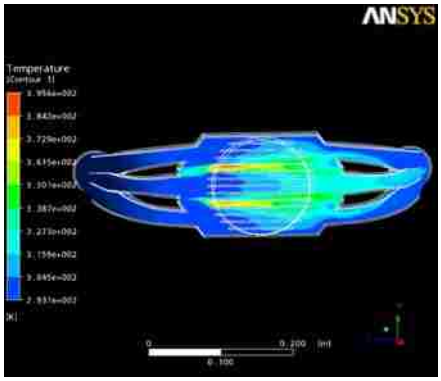

c) Water temperature profile

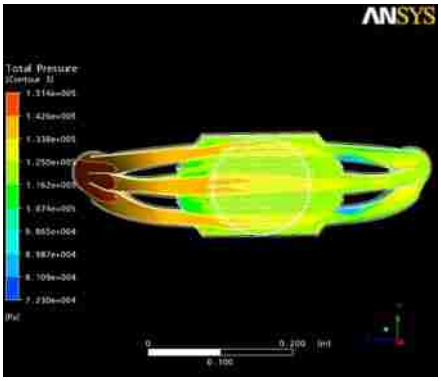

d) Pressure profile

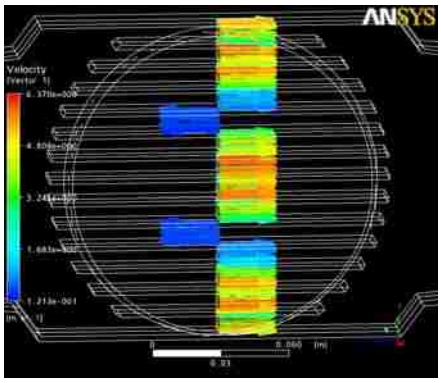

e) Velocity vector profile

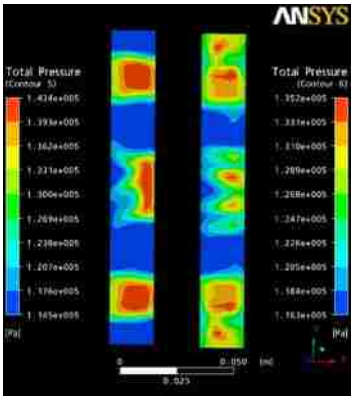

f) Channels inlet-outlet pressure

Figure 3.5 – Initial design 02 results for inlet velocity 3 m/s

A very interesting phenomenon has been identified during the post processing of simulation results. Not only do the low flow channels receive insufficient flow to ensure adequate target cooling, but the direction of the flow in these channels is opposite to the direction in the rest of the channels. Figure 3.5.e) presents the normalized velocity vector profile at the target mid-plane which provides a clear indication of flow reversal. Although this finding seemed to be surprising initially, the pressure distribution profile at the inlet (on the left) and exit (on the right) of the flow channels, Figure 3.5.f), provides additional information that supports this behavior.

While initial design 02 eliminated the flow stagnation point, unequal flow distribution raises concerns regarding adequate management of the target thermal load and maintaining forced convection as the heat transfer mechanism of choice. At the same time, high water inlet velocities require substantial pumping power while operating the cooling system at low pressure level is desirable. The idea of supplying relatively equal mass flow to each channel is explored further since designs with horizontal flow channels show good potential.

3.2.3 Initial Design 03

Based on the results from initial design 02, a new supply and discharge system has been designed that will produce a uniform flow distribution in the channels on the back of the target.

For this design, the water is supplied through a common pipe for all flow channels, flows over the back of the target and is discharged from all channels into one exit pipe.

Circular inlet and outlets are selected to simplify coupling of this system to the pumping and heat removal systems. Also, the geometry of the inlet duct has been chosen such that the inlet area is greater than the total area of the flow channels such that coolant acceleration is achieved. Additionally, the curvature radius for the inlet and outlet ducts provides a smooth change in the flow direction which reduces the pressure losses associated with the fluid flow. The presence of fins, which also serve as flow channel walls, increases the heat transfer from the target to the coolant.

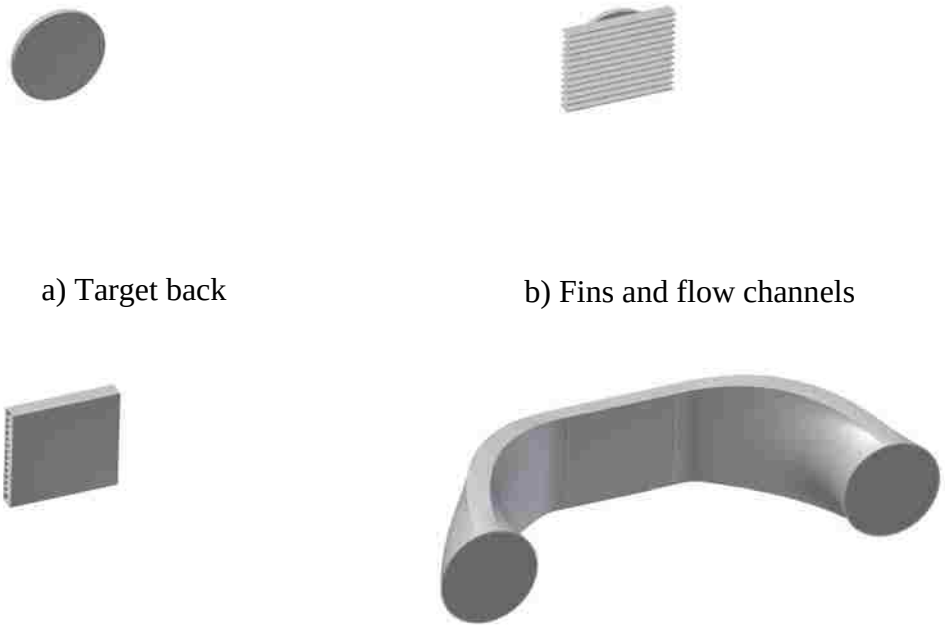

a) Target back

b) Fins and flow channels

c) Water box

d) Complete design

Figure 3.6 – Initial design 03 geometry

The target area subjected to a power input of 180 kW is the same as for initial design 01 and initial design 02. The material used in the simulations of target thermal response is copper and the coolant inlet temperature is 293°K (67.73°F). Simulations have been performed for inlet water velocities of 1, 2 and 3 m/s (3.28, 6.56 and 9.84 ft/s).

Table 3.7 – Initial design 03 characteristics

Parameter	Value
Inlet diameter [mm / inch]	141.0 / 5.551
Inlet area [mm^2 / $inch^2$]	15614.5 / 24.2
Outlet diameter [mm / inch]	141.0 / 5.551
Outlet area [mm^2 / $inch^2$]	15614.5 / 24.2
Fin thickness [mm / inch]	2.0 / 0.0787
Fin height [mm / inch]	20.0 / 0.787
Heated target diameter [mm / inch]	132.4 / 5.213
Heated target area [mm^2 / $inch^2$]	13767.84 / 21.34
Target thickness [mm / inch]	10.8 / 0.425
Water volume [cm^3 / $inch^3$]	5408.2 / 330.03
Metal volume [cm^3 / $inch^3$]	872.61 / 53.25

As presented in Table 3.8 and 3.9, the maximum target temperature for the three water inlet velocities considered is less than the melting temperature of copper.

Table 3.8 – Initial design 03 simulation results (SI units)

Parameter	Inlet velocity [m/s]		
	1	2	3
Maximum target temperature [°K]	938.52	830.15	784.60
Pumping power [W]	262.37	1892.29	5942.70
Maximum water temperature [°K]	319.40	307.20	302.85
Maximum water velocity [m/s]	7.50	14.86	22.18
Coolant mass flow [kg/s]	15.54	31.09	46.63
Minimum system pressure [Pa]	85021.0	40561.5	-
Maximum system pressure [Pa]	128370.0	207278.0	328233.0
Outlet static pressure [Pa]	100000.0	100000.0	100000.0

Table 3.9 – Initial design 03 simulation results (British units)

Parameter	Inlet velocity [ft/s]		
	3.28	6.56	9.84
Maximum target temperature [°F]	1229.67	1034.6	952.61
Pumping power [hp]	0.3518	2.538	7.969
Maximum water temperature [°F]	115.25	93.29	85.46
Maximum water velocity [ft/s]	24.606	48.753	72.769
Coolant mass flow [lb/s]	34.26	68.542	102.8
Minimum system pressure [psi]	12.331	5.883	-
Maximum system pressure [psi]	18.618	30.063	47.606
Outlet static pressure [psi]	14.5	14.5	14.5

The maximum water temperature is less than the boiling temperature over the entire fluid domain. One of the disadvantages of this design is the high pumping power required to maintain relatively large mass flows through the cooling channel. Additional issues, such as vibrations and erosion, may arise from high maximum water velocity on its path through the cooling channels.

The simulations revealed flow patterns which were not obvious when the initial design 03 geometry was originally conceived. As mentioned above, a high inlet area is beneficial because it allows a relatively small and equally distributed inlet velocity to be accelerated to values that ensure adequate target cooling. The outlet duct was constructed symmetrically to the vertical mid plane and, consequently, the outlet has the same area as the inlet.

Due to high velocity gained through acceleration, the curvature of the outlet duct and the high area of the outlet duct, the water velocity in the region starting from the flow channels exit to the outlet does not present a uniform distribution over the entire flow area. Also, the pressure distribution in this region is skewed such that a high pressure domain is located closer to the outward wall of the outlet flow duct and the low pressure domain establishes inwards.

The distorted pressure profile propagates towards the outlet creating favorable conditions for the formation of vortexes at the outlet. Development of this phenomenon in the vicinity of an outlet boundary should be avoided in CFD simulation because it reduces

solution accuracy, increases the computational effort and the uncertainty related to the flow conditions in the domain of interest.

Initial design 03 provided the opportunity to observe relevant phenomena for future design improvement. Two important remarks, which will guide the approach to the final design, need to be highlighted. First, a reduction in the outlet area would eliminate the formation of vortexes at the outlet with beneficial effects on the ANSYS CFX-Solver performance and overall solution convergence.

Second, it has been observed that the most important factor in the heat transfer through the target is the thermal resistance of the material. In order to reduce it, the total target thickness has to be reduced. So far, copper was the material of choice due to its high thermal conductivity. On the other hand, molybdenum is the recommended material for generating a high intensity x-ray beam. Although it has a smaller thermal conductivity than copper, molybdenum's superior melting point compensates for this drawback. Thus, the final target designs will be made entirely from molybdenum and will integrate the observations presented so far. Figure 3.7 illustrates the model behavior outlined above.

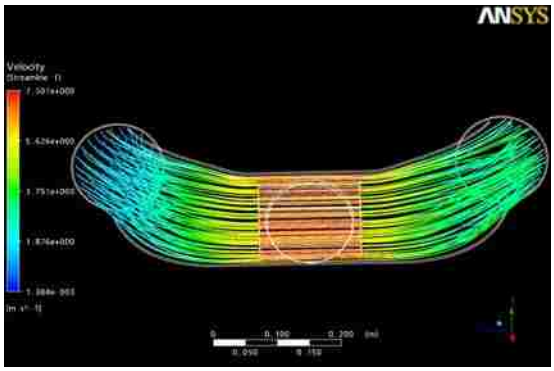

a) Velocity streamline

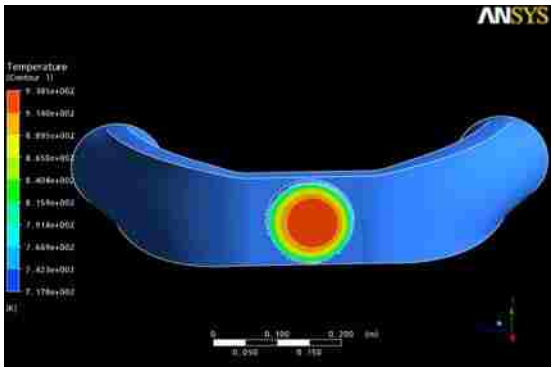

b) Target temperature profile

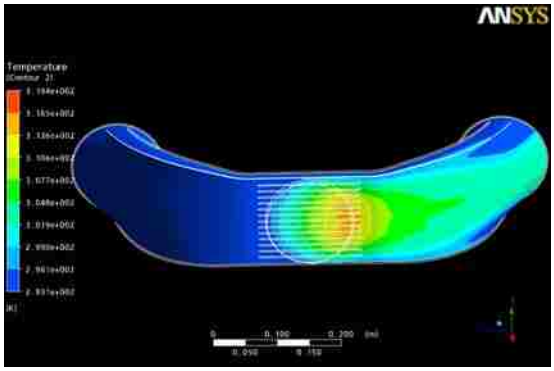

c) Water temperature profile

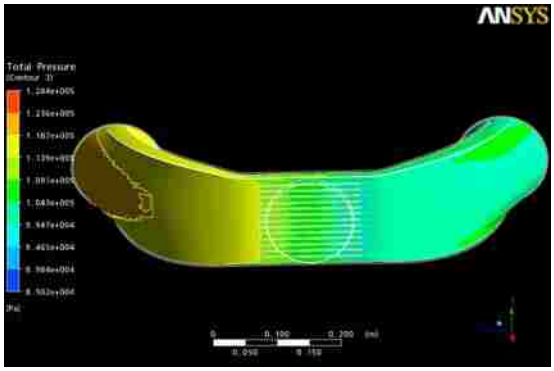

d) Pressure profile

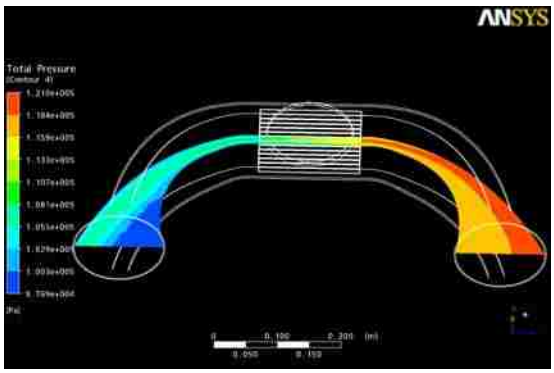

e) Inlet-outlet pressure profile

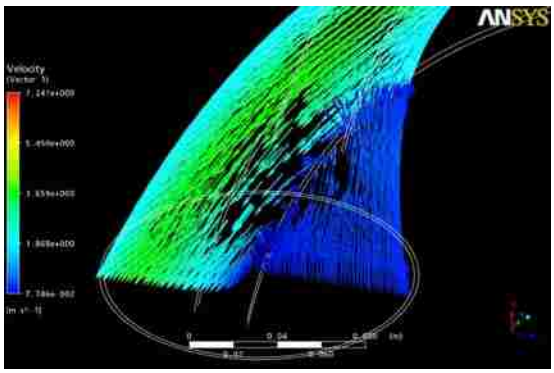

f) Velocity vector profile at outlet

Figure 3.7 – Initial design 03 results for inlet velocity 1 m/s

3.3 Final Design

This chapter is dedicated to the detailed presentation of the final design adopted in this study as the most effective solution to complete thermal management of wide beam area x-ray sources. The final design incorporates the improvements drawn from the earlier designs and takes advantage of the CFD modeling experience and insight gained during these studies.

The information presented in this section is structured in four parts. The first part deals with the geometry design description and material properties. The second part provides information about the mesh and meshing techniques employed. The CFD model construction details are unveiled in the third part. Finally, a roadmap that offers a clear and concise design performance evaluation is shown in the fourth part.

3.3.1 Geometry

The geometry for the final design is inspired by the work done during the development of initial design 03. Additionally, several important features which distinguish the final design from the initial design and provide significant improvements in terms of cooling performance have been incorporated. The final design geometry is presented in Figure 3.8 – 3.11.

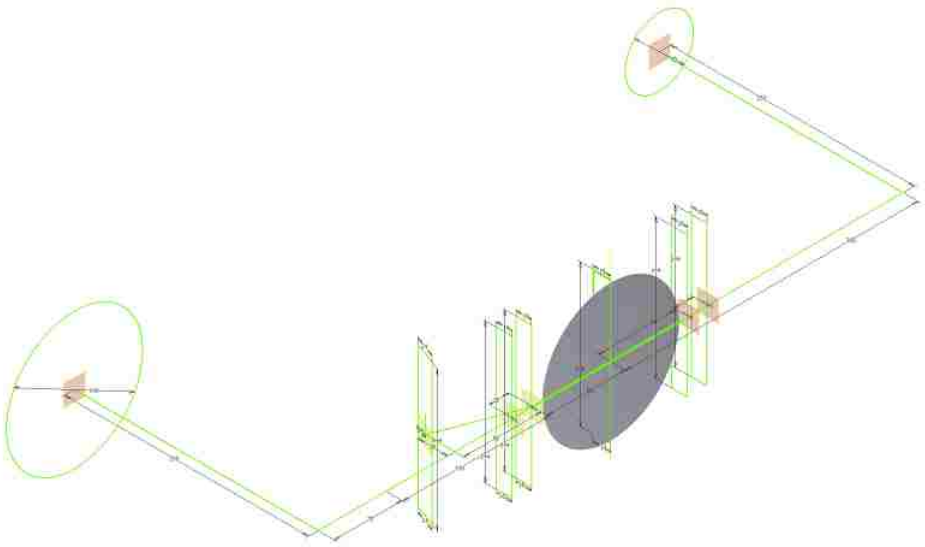

Figure 3.8 – Final design geometry – Target front

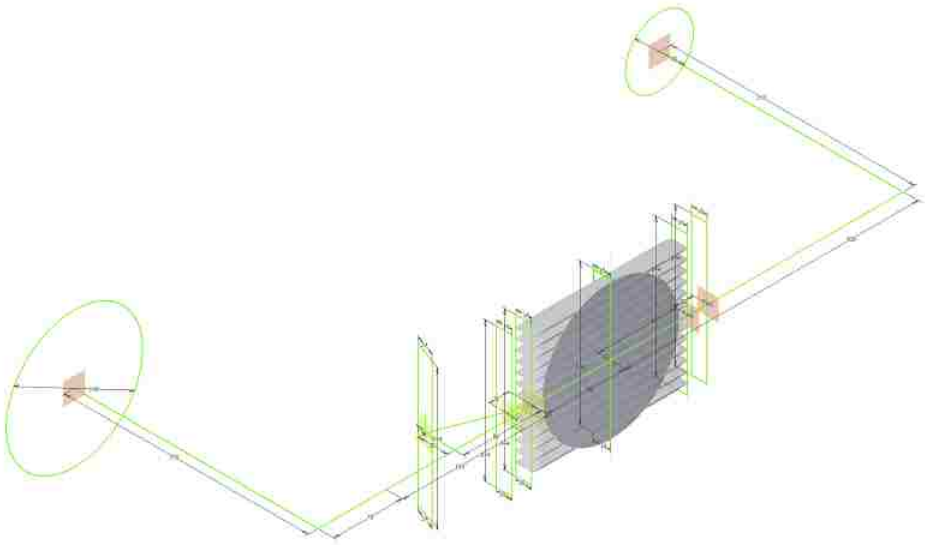

Figure 3.9 – Final design geometry – Fins

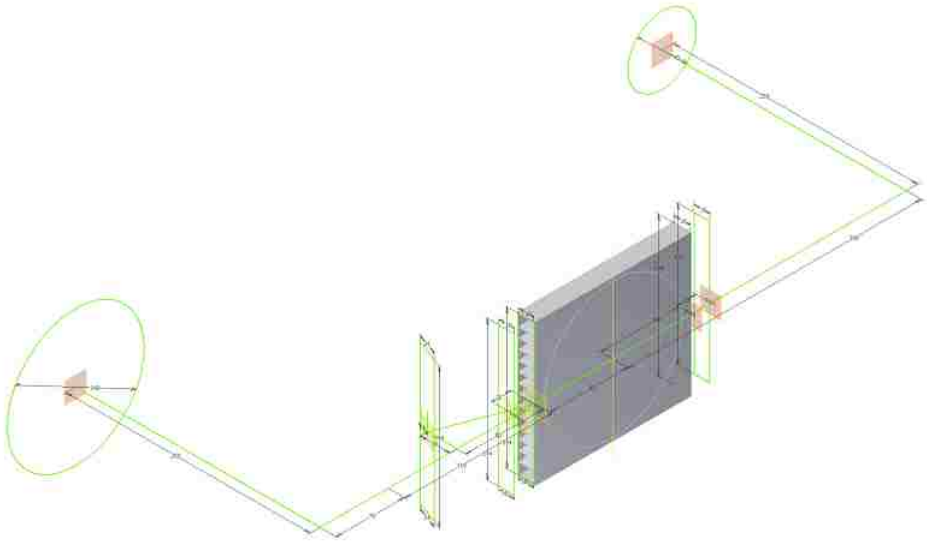

Figure 3.10 – Final design geometry – Cooling channels

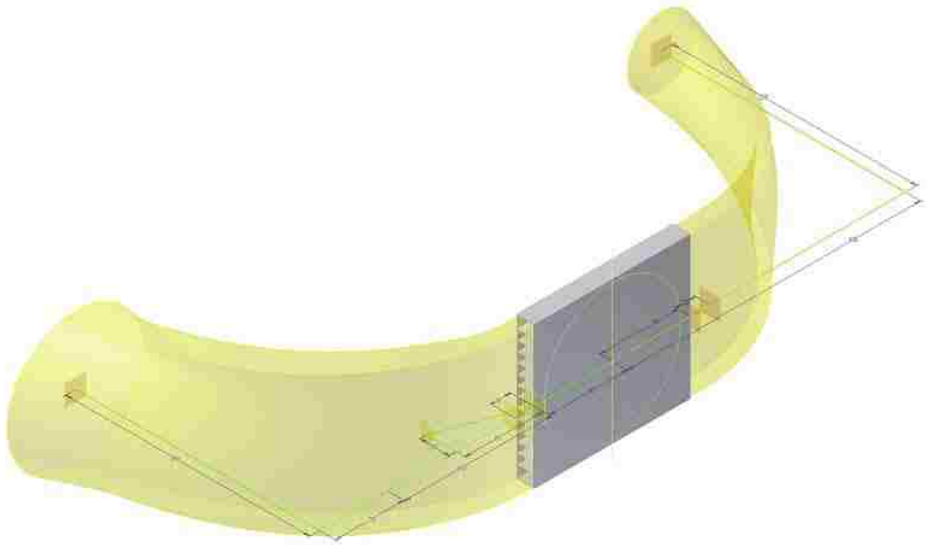

Figure 3.11 – Final design geometry – Complete design

The final design comes in three distinct versions which differ only in total target wall thickness. Figure 3.12 presents a sectional view and highlights of the three versions of the final design.

As seen in Figure 3.11, the coolant enters from the left side, through the larger inlet area, flows through the inlet duct, is distributed through the flow channels, sweeps the back of the target and is discharged through the outlet duct and the smaller outlet area. The heat flux is imposed on the front area of the target, depicted in Figure 3.8. Table 3.10 lists the most important geometrical features of the final design.

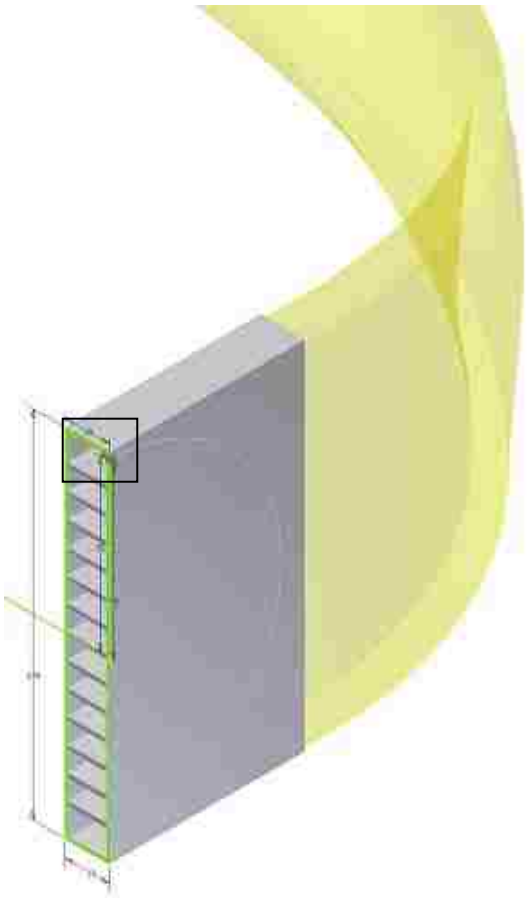

a) Final design transversal view

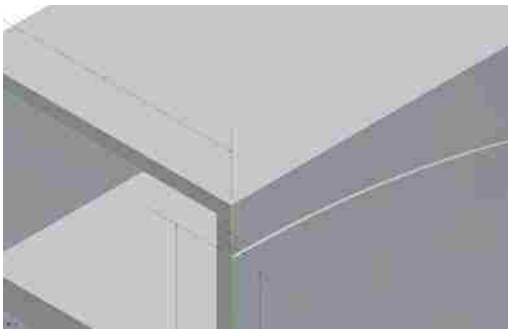

b) Final design ver.01

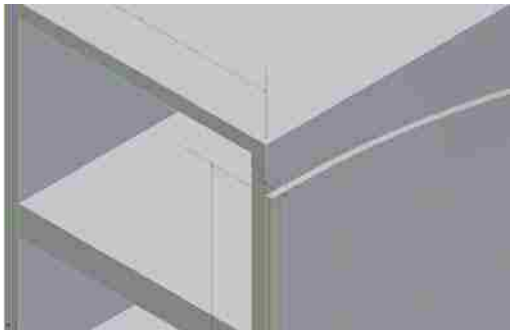

c) Final design ver.02

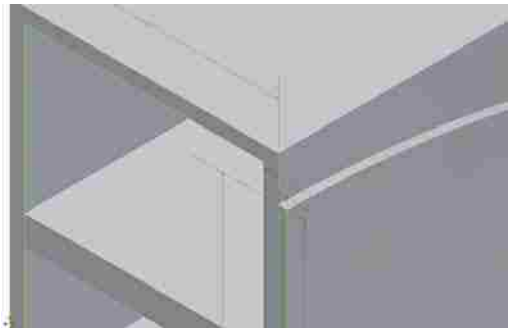

d) Final design ver.03

Figure 3.12 – Final design sectional view and highlights

Table 3.10 – Final design features

Parameter	Design version		
	01	02	03
Inlet diameter [mm / inch]	140.0 / 5.51	140.0 / 5.51	140.0 / 5.51
Inlet area [mm^2 / $inch^2$]	15393.8 / 23.9	15393.8 / 23.9	15393.8 / 23.9
Fin thickness [mm / inch]	2.0 / 0.0787	2.0 / 0.0787	2.0 / 0.0787
Fin height [mm / inch]	16.0 / 0.63	16.0 / 0.63	16.0 / 0.63
Fin length [mm / inch]	160.0 / 6.3	160.0 / 6.3	160.0 / 6.3
Fin spacing [mm / inch]	10.0 / 0.394	10.0 / 0.394	10.0 / 0.394
Water box wall thickness [mm / inch]	1.0 / 0.0394	1.0 / 0.0394	1.0 / 0.0394
Cooling channel height [mm / inch]	16.0 / 0.63	16.0 / 0.63	16.0 / 0.63
Cooling channel width [mm / inch]	8.0 / 0.315	8.0 / 0.315	8.0 / 0.315
Heated target diameter [mm / inch]	140.0 / 5.51	140.0 / 5.51	140.0 / 5.51
Heated target area [mm^2 / $inch^2$]	15393.8 / 23.9	15393.8 / 23.9	15393.8 / 23.9
Target wall thickness [mm / inch]	0.2 / 0.00787	0.4 / 0.015	0.6 / 0.023
Total target thickness [mm / inch]	1.2 / 0.0472	1.4 / 0.0551	1.6 / 0.063
Outlet diameter [mm / inch]	70.0 / 2.76	70.0 / 2.76	70.0 / 2.76
Outlet area [mm^2 / $inch^2$]	3848.45 / 5.97	3848.45 / 5.97	3848.45 / 5.97
Water volume [cm^3 / $inch^3$]	3530.3 / 215.4	3530.3 / 215.4	3530.3 / 215.4
Metal volume [cm^3 / $inch^3$]	116.3 / 7.1	119.3 / 7.28	122.43 / 7.47

The material used for the final target design is molybdenum. Since this material is not provided in the ANSYS materials database, it has to be defined by the analyst. The properties required by ANSYS are listed in Table 3.11, [11].

Table 3.11 – Molybdenum properties

Thermodynamic state	Solid
Property	Value
Molar mass [g/mol]	95.94
Density [g/cm^3]	10.22
Specific heat capacity [kJ/kg·°K]	0.255
Thermal conductivity [W/m·°K]	138.0

3.3.2 Mesh

The mesh for the final design is obtained based on the geometry constructed using Autodesk Inventor Professional 2008. An individual mesh has been created for each design version. ANSYS ICEM CFD has been used to create the model meshes, as it integrates advanced geometry acquisition, mesh generation, mesh optimization and post-processing tools, [12]. ANSYS ICEM CFD mesh generation capabilities include multiblock structured, unstructured hexahedral, unstructured tetrahedral, hybrid meshes comprising hexahedral, tetrahedral, pyramidal and/or prismatic elements, quadrilateral and triangular surface meshes. This project uses the unstructured tetrahedral (Tetra) mesh for the volumes and triangular mesh for surfaces.

Tetra mesh employs several meshing techniques to fill the volume of interest with tetrahedral elements and generate a surface mesh on the object surface. The positions of edges and vertices in the mesh are determined based on the prescribed points and curves loaded from the geometry file. To improve mesh quality, Tetra incorporates a powerful smoothing algorithm, as well as capability to provide local adaptive mesh refinement and coarsening. The steps required to obtain a mesh are presented further. It should be emphasized that the accuracy of the CFD model and the rapid convergence of the CFD solution are strongly dependent on the successful generation of a quality mesh.

The geometry repair/clean up is the first step in generating a Tetra mesh. This ensures that the geometry is free of any flaws that would inhibit the mesh creation. To create a mesh, Tetra requires that the model is a closed volume. If there are any holes (gaps or missing surfaces) in the geometry larger than the local tetras, the meshing algorithm will be unable to close the volume and to complete the mesh creation. It is the responsibility of the analyst to fix the surface data and to eliminate these holes.

The second step requires that the geometry details be preserved while the mesh is created. In addition to a closed set of surfaces that encloses the volume of interest, Tetra requires curves and points where hard features, such as hard angles and corners, to be captured in the mesh. Thus, the mesh provides accurate representation of the initial geometry.

In order to produce an optimal mesh, it is very important that all surfaces and curves have the proper tetra sizes assigned to them. Inadequate assignments may create finer mesh

elements in regions of secondary importance, while in the areas of interest coarser mesh may not allow the investigated phenomena to be well represented and understood.

The Tetra mesh creation uses the Octree mesh method, [12] and [13], which is based on the spatial subdivision algorithm that ensures refinement of the mesh where necessary, but maintains larger elements where possible, allowing for faster computation. Once the "root" tetrahedron, which encloses the entire geometry, has been initialized, Tetra subdivides the root tetrahedron until all the element size requirements are met. The subdivision is performed such that elements sharing a face or an edge would not be different in size by more than a factor of 2. After the subdivision process is complete, Tetra makes the mesh conformal. This ensures that each pair of adjacent elements will share an entire face. At this point, the mesh does not respect the given geometry. Next, the mesher rounds the nodes of the mesh to the prescribed points, prescribed curves or model surfaces. Tetra cuts away all the mesh that can not reach a material point from the geometrical domain. Finally, the mesh is smoothed by moving nodes, merging nodes, swapping edged and, if required, by deleting bad elements.

Target mesh generation for each of the final design versions strived to achieve a good balance between the quality of the mesh and the size of the mesh. A high quality mesh is of outmost importance for ensuring adequate geometry representation, rapid simulation convergence and reliable numeric output. In the same time, keeping the total number of mesh elements to a reasonable value to decrease memory, storage space requirements and total simulation time presented a difficult challenge. Table 3.12 provides a concise outline of the mesh characteristics for each design version analyzed.

Table 3.12 – Final design mesh characteristics

Part	Final design		
	01	02	03
Inlet			
Triangles	2272	2652	2622
Nodes	1137	1327	1312
Outlet			
Triangles	610	678	676
Nodes	306	340	339
Heated target area			
Triangles	8359	9543	10242
Nodes	4300	5261	5237
Molybdenum			
Tetrahedrons	211343	210020	237427
Nodes	59076	58746	63647
Faces	99416	99066	100922
Water			
Tetrahedrons	870122	863279	860338
Nodes	175237	173910	173392
Faces	113910	113392	113448
Total			
Tetrahedrons	1081465	1073299	1097765
Nodes	234313	232656	237039
Faces	213326	212458	214370

3.3.3 CFD Model

The development of each final design CFD model starts by defining a blank project and loading the appropriate mesh. Once ANSYS CFX-Pre finishes the mesh loading, the first step is to define the domains based on the geometry contained in the mesh. A domain usually consists of a closed geometrical volume which either can be solid, fluid or porous.

For the purpose of this research, two domains have been defined: one solid (molybdenum target) and one fluid (water). The preprocessor automatically creates an interface between the solid and the fluid domain in order to allow heat transfer to be calculated. The flow conditions at the limits of the fluid domain are specified through boundary conditions. For the water inlet, an Inlet boundary condition has been specified and for the water outlet an Outlet boundary is imposed.

To model the heat addition to the target, a Wall type boundary condition is employed for the heated target area. The heat flux on the heated target area can be specified either as a constant value or as a variable which stores spatial heat flux distribution. Details on the boundary conditions for the fluid and solid domain are available in Table 3.13.

As presented in Chapter 2, the turbulence model of choice for the simulation of target behavior is the k-epsilon model. A couple of remarks will be made regarding the convergence and solver options selected to enhance the numerical solution resolution. Also, selected solver convergence plots can be seen in Appendix B.

Table 3.13 – Model boundary condition details

Boundary condition	Details			
Inlet	Flow regime: Subsonic	Mass and momentum: Normal speed	Turbulence: Medium	Heat transfer: Temperature
Outlet	Flow regime: Subsonic	Mass and momentum: Average static pressure	Pressure averaging: Average Over Whole Outlet	-
Wall	Heat transfer: Heat flux in	-	-	-

A solution to a CFD problem is obtained by resolving various equations using the appropriate boundary conditions and models. At any moment during the calculation, each equation will not be completely satisfied, and the “residual” of an equation provides a measure of the difference between the left-hand-side of the equation and the right-hand-side of the equation at any point in space. If the solution is exact, the residual is zero meaning that each relevant finite volume equation is satisfied precisely. This is not the case because the equations model the physics approximately.

However, if a solution is converging, residuals should decrease with successive iterations. A plot of the residuals for each equation during the simulation provides a measure of how well the solution is converging. One way to quantify the solution convergence is to plot the Root Mean Square residual.

The RMS residual is obtained by taking all the residuals throughout the domain, squaring them, taking the mean, and then taking the square root of the mean. For any simulation in this study, the maximum RMS residual is less than $1 \cdot 10^{-5}$. These provisions are necessary to ensure reasonable numerical accuracy for the results presented herein.

ANSYS CFX-Solver has two classes of executables: default (single precision) and double precision. Double precision Solver executables store basic floating point numbers as 64 bit words. These executables permit more accurate numerical mathematical operations. Double precision accuracy might be needed if the computational domain involves a huge variation in grid dimensions, aspect ratio, pressure range, etc. The double precision Solver has been the standard choice for all simulations performed as part of this thesis.

3.3.4 Evaluation Roadmap

To confirm that the final design meets the requirements specified in Section 3.1, an evaluation roadmap has been envisioned. The roadmap ensures a thorough assessment of the target performance and provides a solution space based on the significant design and operation parameters. The roadmap consists of two sections: simulation and post-processing. Figure 3.13 provides an overview of each section contents. Additionally, detailed explanations for the steps contained in each section are provided as required.

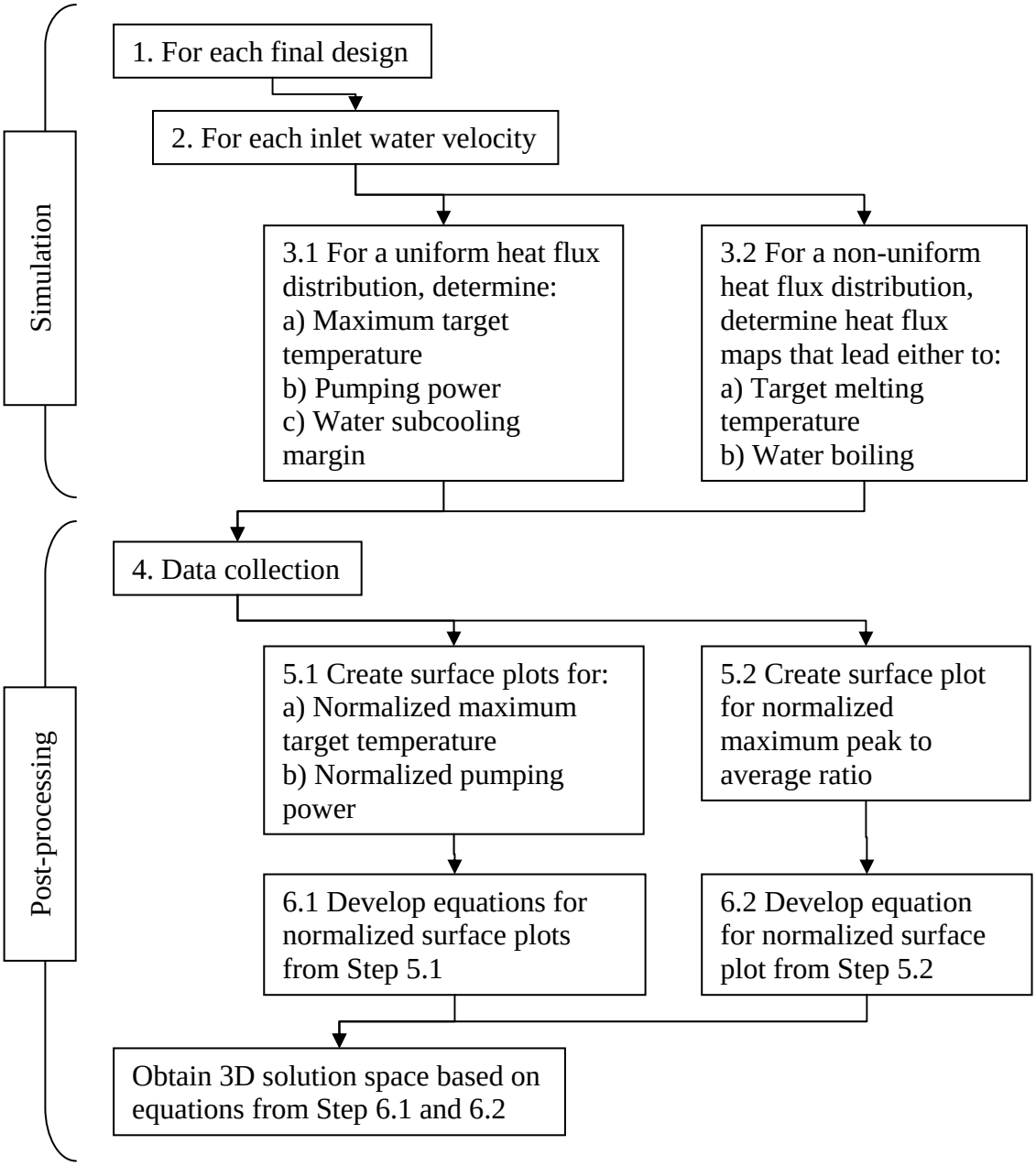

Figure 3.13 – Final design evaluation roadmap

As previously mentioned, three versions of the final design have been investigated, each corresponding to a total target thickness of 1.2 mm (0.0472 inch), 1.4 mm (0.0551 inch) and 1.6 mm (0.063 inch). For each version, water inlet velocity has been varied from 0.6 m/s (1.97 ft/s) to 1.2 m/s (3.94 ft/s) in increments of 0.1 m/s (0.328 ft/s). As mentioned in Figure 3.13, Step 3.1 and 3.2, uniform heat flux and non-uniform heat flux distributions have been imposed as boundary conditions on the heated target area for each combination of wall thickness and water inlet velocity. For simulations performed at Step 3.1, the uniform heat flux is determined based on a maximum target power of 180 kW and a target area of 15393.8 mm^2 (23.9 $inch^2$) which yields $11.693 \cdot 10^6$ W/m^2 ($3.707 \cdot 10^6$ $Btu/h \cdot ft^2$).

Non-uniform heat flux distributions arise from the practical difficulty of generating a uniform electron beam. There are two parameters that identify a non-uniform distribution. The first one is the average heat flux of the distribution, which for the purpose of this study is maintained at the same value as the uniform distribution value. The second parameter is the peak to average ratio which is obtained by dividing the highest heat flux value by the average heat flux value for a distribution. The method for constructing a non-uniform distribution is presented further.

First, it is required to select a function that provides a smooth variation from low to high values; its shape can be changed by modifying one of its parameters while the average value remains constant over the range of interest. These characteristics are exhibited by a family of continuous probability distributions, most precisely the Gaussian distributions. From that family, the normal distribution has been selected. One of the best known visual

representations of the normal distribution is provided by the continuous probability density function (PDF), as seen in Figure 3.14.

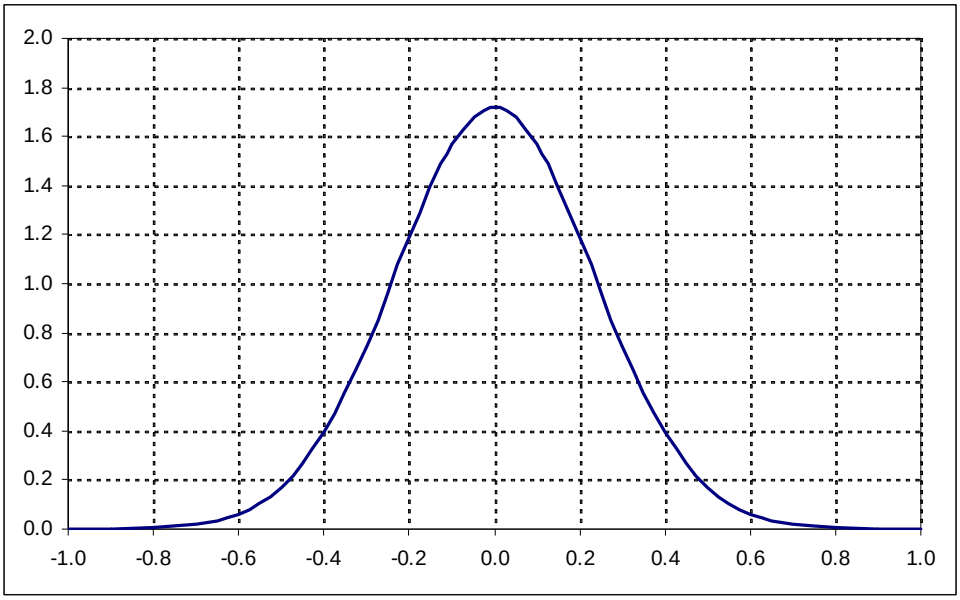

Figure 3.14 – Continuous probability density function for normal distribution

The continuous probability density function is given by:

$$f(x,\mu,\sigma)=\frac{1}{\sigma\sqrt{2\pi}}e^{-\frac{(x-\mu)^2}{2\sigma^2}} \qquad (3.1)$$

where x is the argument of the function, μ is the expected value (mean) and σ represents the standard deviation. To obtain a symmetrical distribution and considering the target center as

the most limiting position for the maximum heat flux value, the expected value of the PDF is set to zero for all distributions herein.

The non-uniform heat flux distribution required as input in ANSYS-CFX has to be provided in the format: X coordinate, Y coordinate, Z coordinate and heat flux value. Because the flux distribution is on a planar surface perpendicular on X-Axis, the X coordinate is constant. Consequently, the problem reduces to generating an n × n matrix of heat flux values – M(i,j), i=1..n, row index, j=1..n, column index, n=21 – which satisfies the following requirements:

- the average value of the elements in the matrix is constant,
- the elements in any row or column follows a normal distribution,
- the matrix has quadrant symmetry, the elements positioned at equal distance left-right from the center column and up-down from the center row have the same value.
- different ratios of the maximum value to the average value have to be obtained by changing a single parameter.

Matrix M generation starts with the creation of the center row, M(11,1..21). The center row is generated using the PDF for a normal distribution with the argument ranging from -1 to 1. The initial value for the standard deviation is chosen randomly, and will be fine tuned later as required. The second step is to create an array of multiplication factors, – F(k,p), k=1..10, row index, p=1, column index – obtained by dividing the maximum center row value by the rest of the elements within the row.

$$F(k,1) = \frac{M(11,11)}{M(11,k)}, k = 1..10 \qquad (3.2)$$

Next, the remaining 20 rows of elements in matrix M have to be calculated. The values for elements in a row are determined by dividing the values from row 11 to the corresponding multiplication factor. For example, M(5,1..21) values are calculated using:

$$M(5,j) = \frac{M(11,j)}{F(5,1)}, j = 1..21 \qquad (3.3)$$

After all the above operations, the elements from matrix M still have the values calculated using the probability density function. By multiplying all the elements by the uniform, average heat flux value, a complete non-uniform heat flux distribution is obtained. From this distribution, a peak to average ratio can be easily determined. There is one parameter of the probability density function which controls the shape and peak to average ratio for any heat flux distribution. This parameter is the standard deviation. A non-uniform heat flux distribution with desired peak to average ratio is obtained through fine tuning the standard deviation value.

Overlapping the heat flux distribution contained in matrix M to the actual target area is the final step of the process. The heated area of the target has a diameter of 140 mm and was divided into 18 equal length segments along both Y and Z coordinates. This creates a 19 by 19 equally spaced square grid of points. Each point corresponds to an element from matrix M. Since the heated target area has a circular shape, there are points that fall outside the contour and these values are discarded. The use of a normal distribution for the heat flux is

beneficial because the heat flux values for the discarded points are very small. Selected heat flux distribution profiles can be seen in Appendix A.

Simulations performed using a uniform heat flux distribution, Figure 3.13 - Step 3.1, provide as output the maximum target temperature, the required pumping power and the water subcooling margin for each case analyzed. The subcooling margin has been calculated as the difference between water saturation temperature corresponding to the minimum total pressure and the maximum water temperature, within the whole fluid domain, obtained from simulation.

For simulations involving non-uniform heat flux distributions, Figure 3.13 - Step 3.2, the purpose was to determine the heat flux shape, uniquely identified by its peak to average ratio, which would produce a maximum target temperature equal to the target melt temperature or would create favorable conditions for localized water boiling (subcooling margin equals to zero). For each target wall thickness and each water inlet velocity, the process is iterative and requires a large number of CFD runs.

The simulation results obtained from Step 3.1 and 3.2 are compiled in a useful form for the second phase of final design evaluation – post-processing. Data tables containing maximum target temperature, pumping power and maximum peak to average ratio as a function of total target thickness and water inlet velocity are developed. These data collections serve as input for Figure 3.13 – Step 5.1 and 5.2. During this step, the variables of interest (maximum target temperature, pumping power and maximum peak to average ratio) are normalized by dividing all values by the maximum value. Thus, a new set of tables is

obtained in which all variables values are between 0 and 1 and their dependence on total target thickness and water inlet velocity is preserved. Based on the normalized tables, surface plots are created to provide a visual representation of the data.

During Step 6.1 and 6.2, the normalized data obtained previously is used to construct three surface equations, each corresponding to maximum target temperature, pumping power and maximum peak to average ratio as a function of total target thickness and water inlet velocity. The intersection of these equations provides the three dimensional solution space for the final design.

Chapter 4 Results

This chapter presents the CFD simulation results of the final design and consists of four parts. The first part will elaborate on the findings resulting from simulations considering the uniform heat flux distribution. The second part will examine the final design response for the case of a non-uniform heat. The construction of design solution space is detailed in the third part. Finally, result analysis is provided in the fourth part.

4.1 Uniform Heat Flux Distribution

As previously mentioned, a uniform heat flux distribution has been considered as part of final target design evaluation. The heat flux value imposed as boundary conditions is $11.693 \cdot 10^6$ W/m^2 ($3.707 \cdot 10^6$ Btu/h·ft^2). The water inlet temperature for all simulations is 293°K (67.73 °F). The target material is molybdenum with a melting temperature of 2890°K (4742.33°F). The pressure drop across the target is determined as the difference between the average inlet pressure and the average outlet pressure. The pumping power associated with the coolant flow is calculated using Eq. (4.1) based on total mass flow, water density and the pressure drop. The average water density used in the Eq. (4.1) is 997 kg/m^3 (62.24 lb/ft^3).

$$P = \frac{\dot{m}}{\rho} \Delta p \qquad (4.1)$$

For each design, simulations have been performed for inlet water velocity ranging from 0.6 m/s (1.97 ft/s) to 1.2 m/s (3.94 ft/s). Tables 4.1 - 4.6 present the results for each design version.

Table 4.1 – Final design ver.01 simulation results (SI units)

Location / Parameter	Water inlet velocity [m/s]						
	0.6	0.7	0.8	0.9	1.0	1.1	1.2
Inlet							
Average pressure [Pa]	112206.0	116304.0	120973.0	126211.0	132018.0	138392.0	145.332.0
Average temperature [°K]	293.15	293.15	293.15	293.15	293.15	293.15	293.15
Outlet							
Average velocity [m/s]	2.4	2.8	3.2	3.6	4.0	4.41	4.81
Average pressure [Pa]	102947.0	104012.0	105241.0	106634.0	108192.0	109913.0	111799.0
Average temperature [°K]	297.49	296.87	296.41	296.05	295.76	295.52	295.33
Maximum target temperature [°K]	801.41	754.94	718.31	688.61	664.01	643.27	625.54
Water domain							
Minimum velocity [m/s]	0.55	0.65	0.75	0.84	0.93	1.03	1.12
Minimum pressure [Pa]	98948.1	98578.3	98155.6	97680.3	97152.3	96571.8	95938.5
Minimum temperature [°K]	293.13	298.13	293.13	293.13	293.14	293.14	293.14

Table 4.1 (continued)

Location / Parameter	Water inlet velocity [m/s]						
	0.6	0.7	0.8	0.9	1.0	1.1	1.2
Water domain							
Maximum velocity [m/s]	5.58	6.5	7.42	8.33	9.25	10.17	11.08
Maximum pressure [Pa]	114051.0	118821.0	124268.0	130389.0	137183.0	144649.0	152787.0
Maximum temperature [°K]	331.38	326.22	322.3	319.22	316.73	314.68	312.96
Mass flow rate [kg/s]	9.2	10.7355	12.2692	13.8028	15.3365	16.8701	18.4038
Pressure drop [Pa]	9259.0	12292.0	15732.0	19577.0	23826.0	28479.0	33533.0
Pumping power [W]	85.44	132.36	193.6	271.03	366.51	481.89	618.99
Subcooling margin [°K]	40.93	45.98	49.79	52.74	55.07	56.95	58.49

Table 4.2 – Final design ver.01 simulation results (British units)

Location / Parameter	Water inlet velocity [ft/s]						
	1.97	2.3	2.62	2.95	3.28	3.61	3.94
Inlet							
Average pressure [psi]	16.3	16.9	17.5	18.3	19.1	20.1	21.1
Average temperature [°F]	68	68	68	68	68	68	68
Outlet							
Average velocity [ft/s]	7.87	9.19	10.5	11.8	13.1	14.5	15.8
Average pressure [psi]	14.9	15.1	15.3	15.5	15.7	15.9	16.2
Average temperature [°F]	75.8	74.7	73.9	73.2	72.7	72.3	71.9
Maximum target temperature [°F]	982.88	899.24	833.29	779.83	735.54	698.22	666.31
Water domain							
Minimum velocity [ft/s]	1.8	2.13	2.46	2.76	3.05	3.38	3.67
Minimum pressure [psi]	14.4	14.3	14.2	14.2	14.1	14.0	13.9
Minimum temperature [°F]	68	68	68	68	68	68	68

Table 4.2 (continued)

Location / Parameter	Water inlet velocity [ft/s]						
	1.97	2.3	2.62	2.95	3.28	3.61	3.94
Water domain							
Maximum velocity [ft/s]	18.3	21.3	24.3	27.3	30.3	33.4	36.4
Maximum pressure [psi]	16.5	17.2	18	18.9	19.9	21	22.2
Maximum temperature [°F]	136.81	127.53	120.47	114.93	110.44	106.75	103.66
Mass flow rate [lb/s]	20.28	23.67	27.05	30.43	33.81	37.19	40.57
Pressure drop [psi]	1.35	1.79	2.29	2.84	3.46	4.13	4.87
Pumping power [hp]	0.1146	0.1775	0.2596	0.3635	0.4915	0.6462	0.8301
Subcooling margin [°F]	73.67	82.77	89.67	94.97	99.17	102.47	105.27

Table 4.3 – Final design ver.02 simulation results (SI units)

Location / Parameter	Water inlet velocity [m/s]						
	0.6	0.7	0.8	0.9	1.0	1.1	1.2
Inlet							
Average pressure [Pa]	112230.0	116336.0	121015.0	126264.0	132083.0	138470.0	145423.0
Average temperature [°K]	293.15	293.15	293.15	293.15	293.15	293.15	293.15
Outlet							
Average velocity [m/s]	2.43	2.84	3.24	3.65	4.06	4.46	4.87
Average pressure [Pa]	103036.0	104131.0	105394.0	106824.0	108423.0	110190.0	112125.0
Average temperature [°K]	297.5	296.88	296.42	296.06	295.77	295.53	295.34
Maximum target temperature [°K]	817.313	771.1	734.676	705.15	680.687	660.111	642.506
Water domain							
Minimum velocity [m/s]	0.56	0.65	0.75	0.84	0.93	1.03	1.12
Minimum pressure [Pa]	98548.2	98038.3	97455.9	96801.0	96073.7	95273.9	94401.4
Minimum temperature [°K]	293.13	293.13	293.13	293.13	293.13	293.14	293.14

Table 4.3 (continued)

Location / Parameter	Water inlet velocity [m/s]						
	0.6	0.7	0.8	0.9	1.0	1.1	1.2
Water domain							
Maximum velocity [m/s]	5.6	6.52	7.44	8.36	9.28	10.19	11.11
Maximum pressure [Pa]	114385.0	119262.0	124824.0	131082.0	138023.0	145649.0	153957.0
Maximum temperature [°K]	330.76	325.67	321.81	318.77	316.33	314.31	312.62
Mass flow rate [kg/s]	9.2021	10.7358	12.2695	13.8032	15.3369	16.8706	18.4043
Pressure drop [Pa]	9194.0	12205.0	15621.0	19440.0	23660.0	28280.0	33298.0
Pumping power [W]	84.86	131.42	192.24	269.14	363.96	478.54	614.67
Subcooling margin [°K]	41.44	46.38	50.08	52.93	55.17	56.95	58.39

Table 4.4 – Final design ver.02 simulation results (British units)

Location / Parameter	Water inlet velocity [ft/s]						
	1.97	2.3	2.62	2.95	3.28	3.61	3.94
Inlet							
Average pressure [psi]	16.3	16.9	17.6	18.3	19.2	20.1	21.1
Average temperature [°F]	68	68	68	68	68	68	68
Outlet							
Average velocity [ft/s]	7.97	9.32	10.6	12.0	13.3	14.6	16.0
Average pressure [psi]	14.94	15.1	15.29	15.49	15.73	15.98	16.26
Average temperature [°F]	75.83	74.71	73.89	73.24	72.72	72.28	71.94
Maximum target temperature [°F]	1011.5	928.31	862.75	809.6	765.57	728.53	696.84
Water domain							
Minimum velocity [ft/s]	1.84	2.13	2.46	2.76	3.05	3.38	3.67
Minimum pressure [psi]	14.29	14.22	14.13	14.04	13.93	13.82	13.69
Minimum temperature [°F]	67.96	67.96	67.96	67.96	67.96	67.98	67.98

Table 4.4 (continued)

Location / Parameter	Water inlet velocity [ft/s]						
	1.97	2.3	2.62	2.95	3.28	3.61	3.94
Water domain							
Maximum velocity [ft/s]	18.37	21.39	24.41	27.43	30.45	33.43	36.45
Maximum pressure [psi]	16.59	17.3	18.1	19.01	20.02	21.12	22.33
Maximum temperature [°F]	135.7	126.5	119.6	114.1	109.7	106.1	103.0
Mass flow rate [lb/s]	20.29	23.67	27.05	30.43	33.81	37.19	40.57
Pressure drop [psi]	1.34	1.77	2.27	2.82	3.44	4.11	4.83
Pumping power [hp]	0.1138	0.1762	0.2578	0.3609	0.4881	0.6417	0.8243
Subcooling margin [°F]	74.57	83.47	90.17	95.27	99.27	102.47	105.07

Table 4.5 – Final design ver.03 simulation results (SI units)

Location / Parameter	Water inlet velocity [m/s]						
	0.6	0.7	0.8	0.9	1.0	1.1	1.2
Inlet							
Average pressure [Pa]	112224.0	116329.0	121006.0	126253.0	132070.0	138455.0	145408.0
Average temperature [°K]	293.15	293.15	293.15	293.15	293.15	293.15	293.15
Outlet							
Average velocity [m/s]	2.43	2.84	3.25	3.65	4.06	4.47	4.87
Average pressure [Pa]	103039.0	104135.0	105399.0	106381.0	108431.0	110200.0	112137.0
Average temperature [°K]	297.52	296.9	296.43	296.07	295.78	295.54	295.35
Maximum target temperature [°K]	829.222	784.001	748.303	719.331	695.304	675.029	657.676
Water domain							
Minimum velocity [m/s]	0.56	0.65	0.74	0.84	0.93	1.02	1.12
Minimum pressure [Pa]	98714.7	98263.9	97749.5	97171.3	96529.2	95823.2	95053.4
Minimum temperature [°K]	293.12	293.12	293.13	293.13	293.13	293.14	293.14

Table 4.5 (continued)

Location / Parameter	Water inlet velocity [m/s]						
	0.6	0.7	0.8	0.9	1.0	1.1	1.2
Water domain							
Maximum velocity [m/s]	5.57	6.49	7.41	8.32	9.24	10.15	11.07
Maximum pressure [Pa]	114248.0	119132.0	124666.0	130886.0	137789.0	145376.0	153644.0
Maximum temperature [°K]	333.12	327.73	323.63	318.77	317.82	315.68	313.89
Mass flow rate [kg/s]	9.2021	10.7358	12.2695	13.8032	15.3369	16.8706	18.4043
Pressure drop [Pa]	9185.0	12194.0	15607.0	19422.0	23639.0	28255.0	33271.0
Pumping power [W]	84.78	131.31	192.07	268.89	363.64	478.11	614.17
Subcooling margin [°K]	39.12	44.39	48.34	53.03	53.80	55.73	57.30

Table 4.6 – Final design ver.03 simulation results (British units)

Location / Parameter	Water inlet velocity [ft/s]						
	1.97	2.3	2.62	2.95	3.28	3.61	3.94
Inlet							
Average pressure [psi]	16.28	16.87	17.55	18.31	19.16	20.08	21.09
Average temperature [°F]	68	68	68	68	68	68	68
Outlet							
Average velocity [ft/s]	7.97	9.32	10.66	11.98	13.32	14.67	15.98
Average pressure [psi]	14.94	15.1	15.29	15.43	15.73	15.98	16.26
Average temperature [°F]	75.87	74.75	73.9	73.26	72.73	72.3	71.96
Maximum target temperature [°F]	1032.9	951.53	887.28	835.13	791.88	755.38	724.15
Water domain							
Minimum velocity [ft/s]	1.84	2.13	2.43	2.76	3.05	3.35	3.67
Minimum pressure [psi]	14.32	14.25	14.18	14.09	14.0	13.9	13.79
Minimum temperature [°F]	67.95	67.95	67.96	67.96	67.96	67.98	67.98

Table 4.6 (continued)

Location / Parameter	Water inlet velocity [ft/s]						
	1.97	2.3	2.62	2.95	3.28	3.61	3.94
Water domain							
Maximum velocity [ft/s]	18.27	21.29	24.31	27.3	30.31	33.3	36.32
Maximum pressure [psi]	16.57	17.28	18.08	18.98	19.98	21.09	22.28
Maximum temperature [°F]	139.95	130.24	122.86	114.12	112.41	108.55	105.33
Mass flow rate [lb/s]	20.29	23.67	27.05	30.43	33.81	37.19	40.57
Pressure drop [psi]	1.34	1.77	2.27	2.82	3.43	4.1	4.83
Pumping power [hp]	0.1137	0.1761	0.2576	0.3606	0.4876	0.6412	0.8236
Subcooling margin [°F]	70.37	79.87	86.97	95.47	96.87	100.27	103.17

Data mining the results presented in Table 4.1 – 4.6, maximum target temperature as function of total target thickness and inlet water temperature is obtained. Similarly, pumping power is correlated with the total target thickness and inlet water temperature. Synthetic data for both dependences are shown in Table 4.7 and 4.8.

Table 4.7 – Maximum target temperature dependence, °K

Water inlet velocity [m/s]	Total target thickness [mm]		
	1.2	1.4	1.6
0.6	801.415	817.313	829.222
0.7	754.948	771.1	784.001
0.8	718.31	734.676	748.303
0.9	688.61	705.15	719.331
1.0	664.007	680.687	695.304
1.1	643.271	660.111	675.029
1.2	625.542	642.506	657.676

Table 4.8 – Pumping power dependence, W

Water inlet velocity [m/s]	Total target thickness [mm]		
	1.2	1.4	1.6
0.6	85.44	84.86	84.78
0.7	132.36	131.42	131.31
0.8	193.60	192.24	192.07
0.9	271.03	269.14	268.89
1.0	366.51	363.96	363.64
1.1	481.89	478.54	478.11
1.2	618.99	614.67	614.17

To create a common ground for comparison between the relationships of maximum target temperature and pumping power with total target thickness and water inlet velocity, the results from Table 4.7 and 4.8 have been normalized by dividing all values by the maximum value. This procedure confines the data to a range from 0 to 1. The output is shown in Table 4.9 and 4.10, while visual representations of normalized data are provided in Figure 4.1 and 4.2.

Table 4.9 – Normalized maximum target temperature dependence

Water inlet velocity [m/s]	Total target thickness [mm]		
	1.2	1.4	1.6
0.6	0.966	0.986	1.000
0.7	0.910	0.930	0.945
0.8	0.866	0.886	0.902
0.9	0.830	0.850	0.867
1.0	0.801	0.821	0.839
1.1	0.776	0.796	0.814
1.2	0.754	0.775	0.793

Table 4.10 – Normalized pumping power dependence

Water inlet velocity [m/s]	Total target thickness [mm]		
	1.2	1.4	1.6
0.6	0.138	0.137	0.137
0.7	0.214	0.212	0.212
0.8	0.313	0.311	0.310
0.9	0.438	0.435	0.434
1.0	0.592	0.588	0.587
1.1	0.779	0.773	0.772
1.2	1.000	0.993	0.992

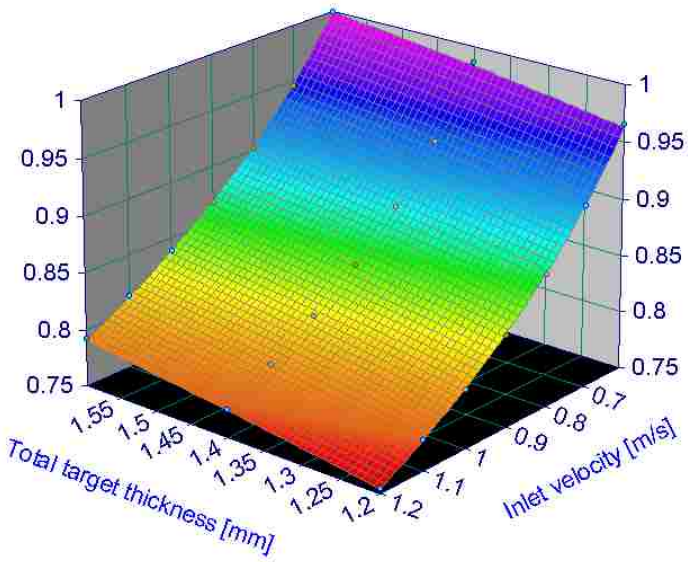

Figure 4.1 – Normalized maximum target temperature dependence

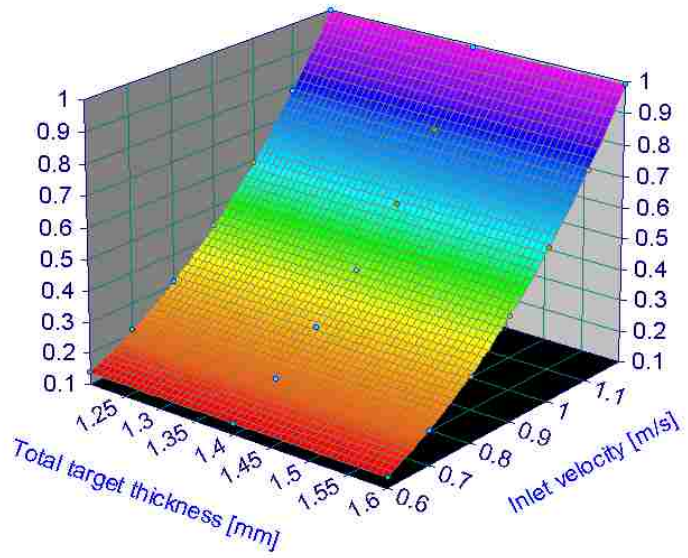

Figure 4.2 – Normalized pumping power dependence

Based on data presented in Table 4.9 and 4.10, general equations of the form z = f(x,y) have been developed for the two dependences, where x represents the total target thickness (mm), y represents water inlet velocity (m/s), and z represents the normalized maximum target temperature or the normalized pumping power. The equations, their coefficients and statistical information regarding the fit accuracy are presented further.

Normalized maximum target temperature equation:

$$z_{temp} = a + be^{-x} + \frac{c}{y^{0.5}} \tag{4.2}$$

where:

a = 0.3582773,

b = -0.36971028,

c = 0.55476743,

Statistical information:

r^2 = 0.99954463, r^2 is the coefficient of determination and provides information about the goodness of fit of a equation,

FitStdError = 0.0016407899, FitStdError is the fit standard error and represents the standard deviation of the fit associated with initial data.

Normalized pumping power equation:

$$z_{power} = e^{a+b\frac{\ln(x)}{x^2}+c\ln(y)} \tag{4.3}$$

where:

a = -0.50353486,

b = -0.15257042,

c = 2.8653701,

Statistical information:

r^2 = 0.99999498,

FitStdError = 0.00064324937.

4.2 Non-uniform Heat Flux Distribution

The challenges posed by the generation of a uniform heat flux on the target surface constitute the primary stimulus behind the investigation of target thermal-hydraulic behavior under a non-uniform heat flux distribution. The heat flux imposed as boundary conditions has a two-dimensional spatial dependence and is obtained as presented in Section 3.3.4. Similar to the uniform heat flux case, the water inlet temperature for all simulations is 293°K (67.73°F). The purpose of the analysis is to determine the heat flux profiles that have the potential of reaching the limiting operating conditions for inlet water velocities ranging from 0.6 m/s (1.97 ft/s) and 1.2 m/s (3.94 ft/s). The limiting operating conditions are the target melting temperature or localized water boiling. Since the heat flux distribution is well characterized by its peak to average ratio, Tables 4.11 – 4.16 present the peak to average ratio for each final design version as a function of inlet water velocity.

Table 4.11 – Final design ver.01 peak to average ratio (SI units)

Parameter	Water inlet velocity [m/s]						
	0.6	0.7	0.8	0.9	1.0	1.1	1.2
Peak to average ratio	4.37	5.35	6.38	7.47	8.08	8.55	9.01
Normal distribution standard deviation	0.33554	0.20197	0.27608	0.255	0.24515	0.2383	0.23213
Subcooling [°K]	0.0947	-0.0008	-0.0046	-0.0468	3.3133	6.9387	10.033
Maximum target temperature [°K]	2265.44	2465.47	2656.41	2854.68	2889.55	2887.53	2889.4
Design limit reached	Water boiling	Water boiling	Water boiling	Water boiling	Maximum target temperature	Maximum target temperature	Maximum target temperature

Table 4.12 – Final design ver.01 peak to average ratio (British units)

Parameter	Water inlet velocity [ft/s]						
	1.97	2.3	2.62	2.95	3.28	3.61	3.94
Peak to average ratio	4.37	5.35	6.38	7.47	8.08	8.55	9.01
Normal distribution standard deviation	0.33554	0.20197	0.27608	0.255	0.24515	0.2383	0.23213
Subcooling [°F]	0.017	-0.001	-0.008	-0.084	5.964	12.49	18.059
Maximum target temperature [°F]	3618.12	3978.18	4321.87	4678.75	4741.52	4737.88	4741.25
Design limit reached	Water boiling	Water boiling	Water boiling	Water boiling	Maximum target temperature	Maximum target temperature	Maximum target temperature

Table 4.13 – Final design ver.02 peak to average ratio (SI units)

Parameter	Water inlet velocity [m/s]						
	0.6	0.7	0.8	0.9	1.0	1.1	1.2
Peak to average ratio	3.55	4.27	5.01	5.79	6.57	7.35	8.17
Normal distribution standard deviation	0.38	0.33971	0.31236	0.29	0.27201	0.25707	0.24379
Subcooling [°K]	-0.0094	0.0551	0.0832	-0.0834	-0.0399	0.0902	-0.0087
Maximum target temperature [°K]	1996.04	2148.97	2292.99	2437.41	2569.3	2691.47	2817.02
Design limit reached	Water boiling	Water boiling	Water boiling	Water boiling	Water boiling	Water boiling	Water boiling

Table 4.14 – Final design ver.02 peak to average ratio (British units)

Parameter	Water inlet velocity [ft/s]						
	1.97	2.3	2.62	2.95	3.28	3.61	3.94
Peak to average ratio	3.55	4.27	5.01	5.79	6.57	7.35	8.17
Normal distribution standard deviation	0.38	0.33971	0.31236	0.29	0.27201	0.25707	0.24379
Subcooling [°F]	-0.017	0.099	0.15	-0.15	-0.072	0.162	-0.016
Maximum target temperature [°F]	3133.2	3408.48	3667.71	3927.67	4165.07	4384.98	4610.97
Design limit reached	Water boiling	Water boiling	Water boiling	Water boiling	Water boiling	Water boiling	Water boiling

Table 4.15 – Final design ver.03 peak to average ratio (SI units)

Parameter	Water inlet velocity [m/s]						
	0.6	0.7	0.8	0.9	1.0	1.1	1.2
Peak to average ratio	3.61	4.41	5.21	6.1	7.0	7.71	8.07
Normal distribution standard deviation	0.37235	0.33395	0.30611	0.28243	0.26346	0.25098	0.2453
Subcooling [°K]	0.2677	-0.0739	0.1159	-0.2052	-0.178	1.4106	4.967
Maximum target temperature [°K]	2048.73	2238.68	2407.98	2601.15	2782.22	2890.51	2889.3
Design limit reached	Water boiling	Water boiling	Water boiling	Water boiling	Water boiling	Maximum target temperature	Maximum target temperature

Table 4.16 – Final design ver.03 peak to average ratio (British units)

Parameter	Water inlet velocity [ft/s]						
	1.97	2.3	2.62	2.95	3.28	3.61	3.94
Peak to average ratio	3.61	4.41	5.21	6.1	7.0	7.71	8.07
Normal distribution standard deviation	0.37235	0.33395	0.30611	0.28243	0.26346	0.25098	0.2453
Subcooling [°F]	0.482	-0.133	0.209	-0.369	-0.32	2.539	8.941
Maximum target temperature [°F]	3228.04	3569.95	3874.69	4222.4	4548.33	4743.25	4741.07
Design limit reached	Water boiling	Water boiling	Water boiling	Water boiling	Water boiling	Maximum target temperature	Maximum target temperature

Similar to the procedure used to obtain fit equations for the normalized dependence of maximum target temperature and pumping power with total target thickness and water inlet velocity, the results from Tables 4.11 – 4.16 are condensed. The resulting data is presented in Table 4.17.

Table 4.17 – Peak to average ratio dependence

Water inlet velocity [m/s]	Total target thickness [mm]		
	1.2	1.4	1.6
0.6	4.37	3.55	3.61
0.7	5.35	4.27	4.41
0.8	6.38	5.01	5.21
0.9	7.47	5.79	6.1
1.0	8.08	6.57	7.0
1.1	8.55	7.35	7.71
1.2	9.01	8.17	8.07

The normalization of data from Table 4.17 is found in Table 4.18. Figure 4.3 illustrates normalized peak to average ratio as function of total target thickness and water inlet velocity.

Table 4.18 – Normalized peak to average ratio dependence

Water inlet velocity [m/s]	Total target thickness [mm]		
	1.2	1.4	1.6
0.6	0.485	0.394	0.401
0.7	0.594	0.474	0.489
0.8	0.708	0.556	0.578
0.9	0.829	0.643	0.677
1.0	0.897	0.729	0.777
1.1	0.949	0.816	0.856
1.2	1.000	0.907	0.896

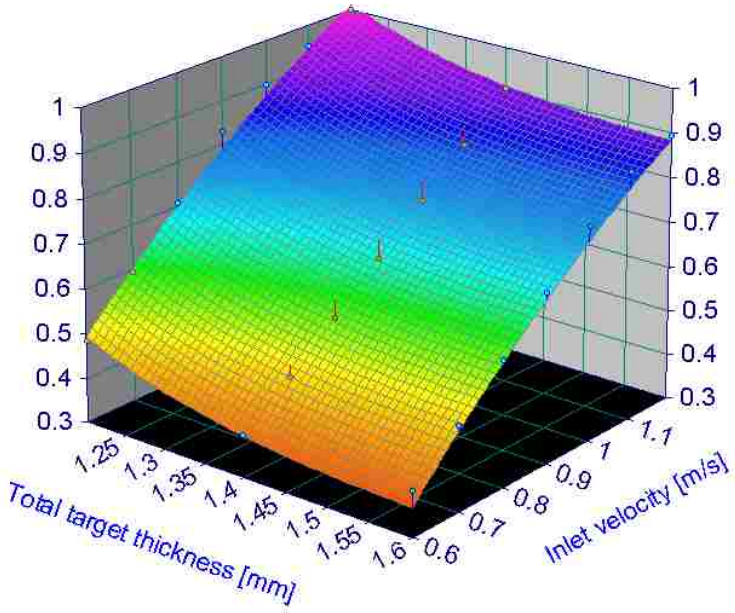

Figure 4.3 – Normalized peak to average ratio dependence

The equation z = f(x,y) for normalized peak to average ratio is given below, where x represents the total target thickness (mm) and y stands for water inlet velocity (m/s).

$$z_{peak} = a + b\frac{\ln(x)}{x^2} + ce^{-y} \quad (4.4)$$

where:

a = 1.9301387,

b = -2.2549277,

c = -2.0978549,

The statistics for Eq. (4.4) are r^2 = 0.97628354 and FitStdError = 0.028173525.

4.3 Design Solution Space

As a way of integrating the simulation results obtained during the uniform and non-uniform heat flux distribution for all the target design versions and operating conditions investigated, a solution space has been envisioned. The solution space is constructed from the intersection of Eq. (4.2), Eq. (4.3) and Eq. (4.4). All equations are a function of total target thickness and water inlet temperature. The parameters span from 1.2 mm (0.0472 inch) to 1.6 mm (0.063 inch) for total target thickness and from 0.6 m/s (1.97 ft/s) to 1.2 m/s (3.94 ft/s) for water inlet velocity.

In Figure 4.4, the red surface corresponds to the normalized maximum target temperature, the blue surface represents normalized pumping power while normalized peak to average ratio is illustrated as the green surface.

For a target design and operating parameters that will position the adopted cooling system solution within the solution space given by the intersection of the three surfaces, reasonable target temperatures are achieved and large non-uniformities in the heat flux shape can be accommodated. Nevertheless, operation within the domain requires substantial pumping power to prevent material melting or coolant boiling. The design solution space does not restrict target design and operation outside its limits. It has been created with the purpose of establishing an enclosed region within which severe heat flux non-uniformity can be properly resolved while feasible target design and operation can still be maintained. If the target illumination can provide reasonable flattened heat flux profiles, then a more relaxed approach can be adopted resulting in a decreased water inlet velocity.

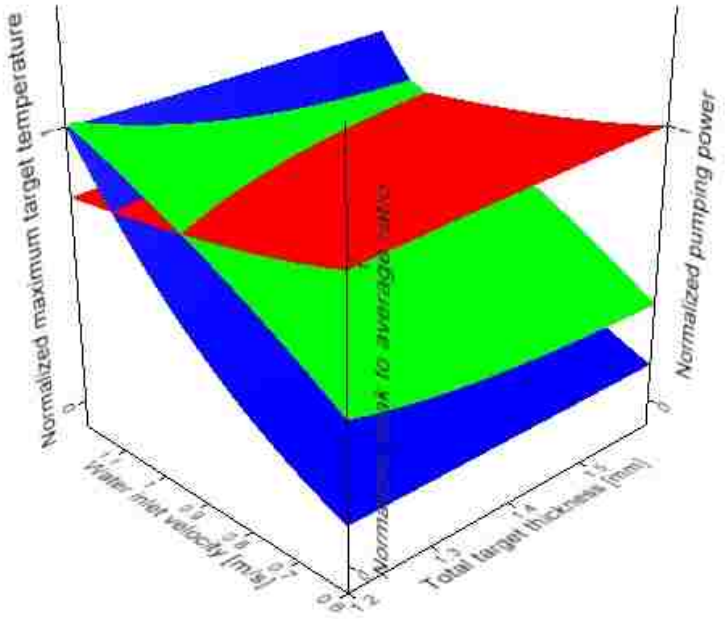

Figure 4.4 – Design solution space

Consequently, the pumping power can be reduced without adversely impacting the target cooling. Important information is obtained through dissection of the design solution space data. Taking different perspectives during this investigation provides a better understanding of the underlying phenomena associated with the final design operation. Section 4.4 presents the findings of this analysis.

4.4 Result Analysis

In order to get a better insight on the information obtained through CFD simulation and from the construction of the design solution space, JMP, a powerful interactive statistics and graphics software package has been employed. The first analysis performed is profiling.

Profiling is used to visualize a response surface with more input factors and one output factor by showing vertical slices across each factor while holding other factors constant. This type of analysis is helpful in determining the relation between the inputs and the output. For the purpose of this study, the response surfaces are maximum target temperature, pumping power and maximum peak to average ratio. The factors are total target thickness and water inlet velocity. The profiler for maximum target temperature is presented in Figure 4.5.

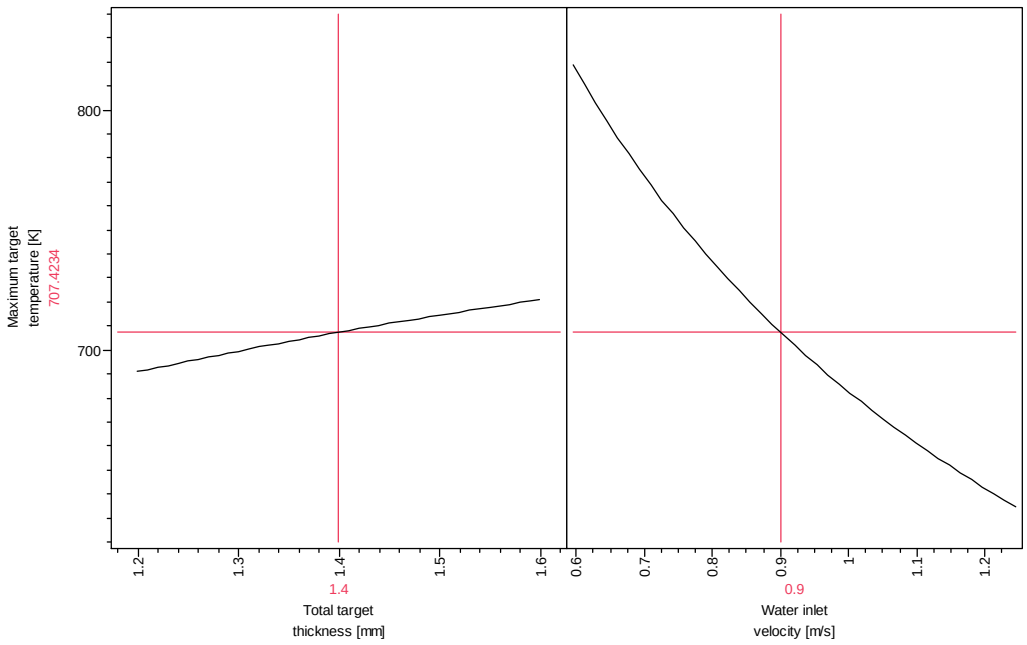

Figure 4.5 – Maximum target temperature profiler

The maximum target temperature profiler from Figure 4.5 offers plenty of information. The right plot relates the maximum target temperature to the water inlet velocity for a constant target thickness. It can be observed that maximum target temperature dependence with target thickness is not very significant compared with the strong dependence exhibited for the water velocity. While maintaining total target thickness constant, the change of water inlet velocity from 0.6 m/s (1.97 ft/s) to 1.2 m/s (3.94 ft/s) will shift the left plot line downwards, from high temperatures to low temperatures without changing the line shape. The magnitude of the change in target temperature is given by the

difference between temperatures corresponding to the water velocity dependence plot extremities.

Similarly, if a constant inlet water velocity is set, the change of total target thickness from 1.2 mm (0.0472 inch) to 1.6 mm (0.063 inch) will cause the right plot line to shift upwards. The magnitude of the shift is equal to the difference between the target temperature corresponding to thickest and, respectively, the thinnest final design version.

Increasing total target thickness causes the thermal resistance to go up and reduces heat transfer efficiency. The direct consequence is a high target temperature. On the other hand, a higher water inlet velocity enhances forced convection and keeps target temperature within reasonable limits.

The maximum target temperature profiler is a versatile tool in understanding the relationship between design parameters, operating conditions and satisfying design requirements. It also provides an easy way of calculating target temperature for any combination of target thickness and water velocity.

The examination of the pumping power profiler, shown in Figure 4.6, provides several important observations. As expected, the pumping power dependence on total target thickness is negligible. As the inlet water velocity increases, a strong boost in the pumping power can be seen. If total target thickness is set to a particular value, increasing the velocity from 0.6 m/s (1.97 ft/s) to 1.2 m/s (3.94 ft/s) results in a shift upwards of the line in the left plot. It is worth noting that this behavior is opposite to the one observed during the analysis of the maximum target temperature profiler.

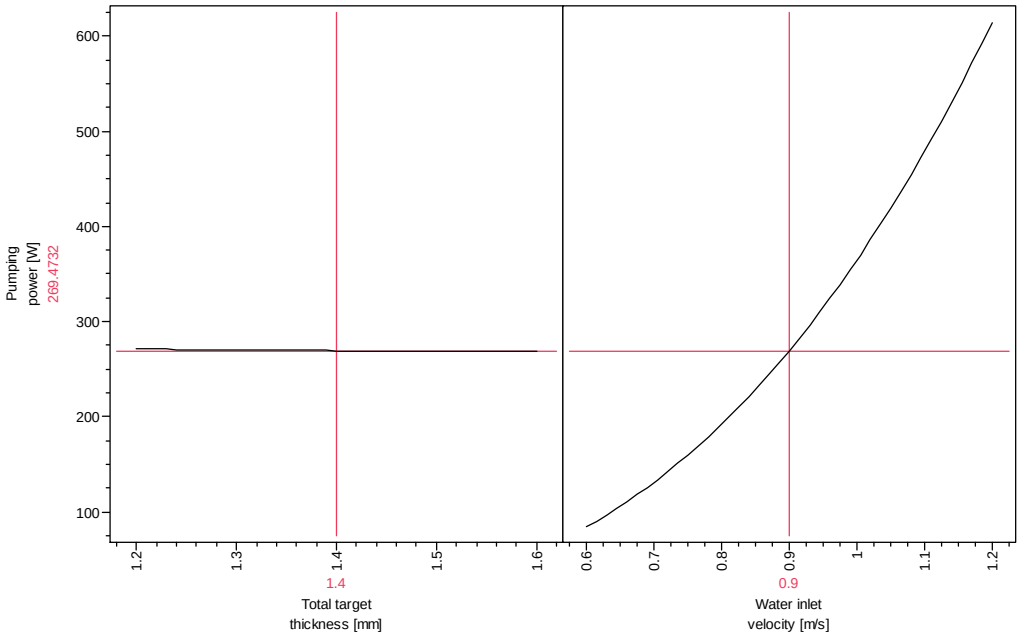

Figure 4.6 – Pumping power profiler

Figure 4.7 presents the peak to average ratio profiler. The peak to average ratio displays a moderate dependence on total target thickness, while a strong dependence on water inlet velocity is demonstrated. Keeping the total target thickness constant, a change in water inlet velocity from 0.6 m/s (1.97 ft/s) to 1.2 m/s (3.94 ft/s) shifts the left plot line from low to high peak to average ratio values. On the other hand, contrary to the behavior encountered during the analysis of the maximum target temperature profiler, increasing total target thickness for a constant water inlet velocity moves down the right plot line, thus decreasing the peak to average value. The maximum vertical shift for one plot line equals the difference between the top and the bottom value of the other plot line.

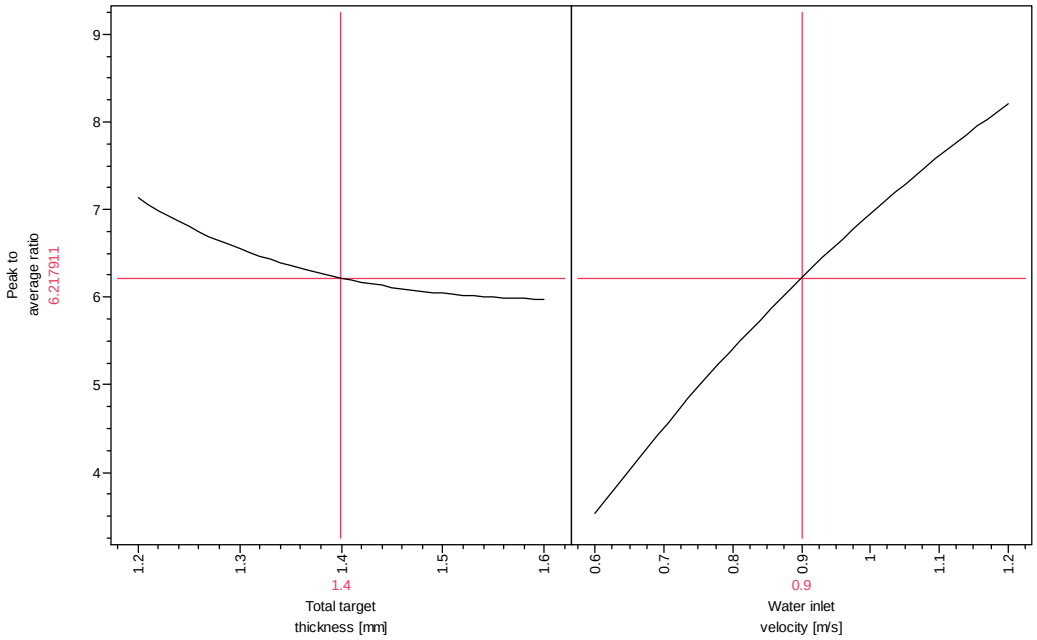

Figure 4.7 – Peak to average ratio profiler

Result analysis has dealt so far with establishing and explaining dependences between design criteria and design / operation parameters. From a practical perspective, the use of simple, yet powerful, graphical representations that provide numerical evaluation of maximum target temperature, pumping power and peak to average ratio is more suitable. Consequently, a different analysis approach is considered which involves contour plots. The contour plots are constructed for variables of interest as function of total target temperature and water inlet velocity. Figure 4.8 presents the contour plot for maximum target temperature.

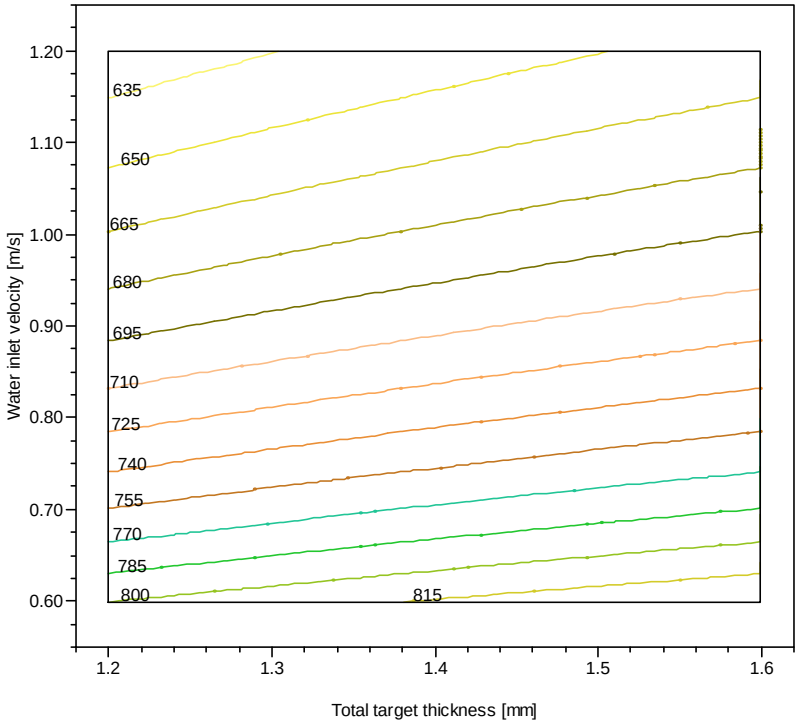

Figure 4.8 – Maximum target temperature contour plot

Figure 4.8 permits a quick evaluation of target temperature based on any combination of parameters. Each line corresponds to a constant target temperature, known as an isothermal. For a parameter combination which renders a point positioned within two isothermals, simple linear interpolation provides a reasonable approximation for the target temperature. It can be seen that maximum target temperature increases with target thickness and decreases with water inlet velocity.

The contour plot for pumping power is shown in Figure 4.9. As it can be seen, the pumping power is primarily a function of water inlet velocity and is virtually independent of total target thickness.

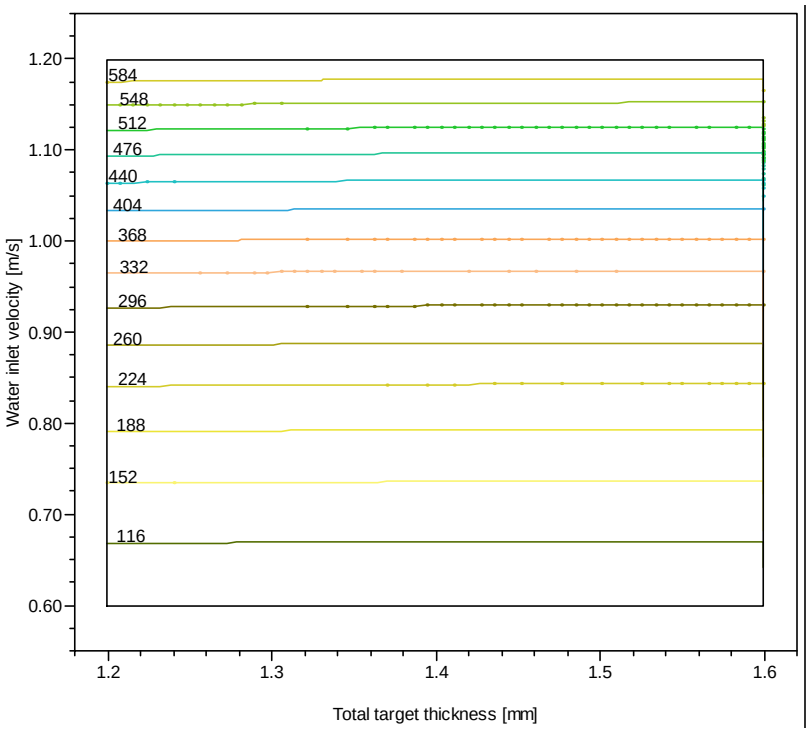

Figure 4.9 – Pumping power contour plot

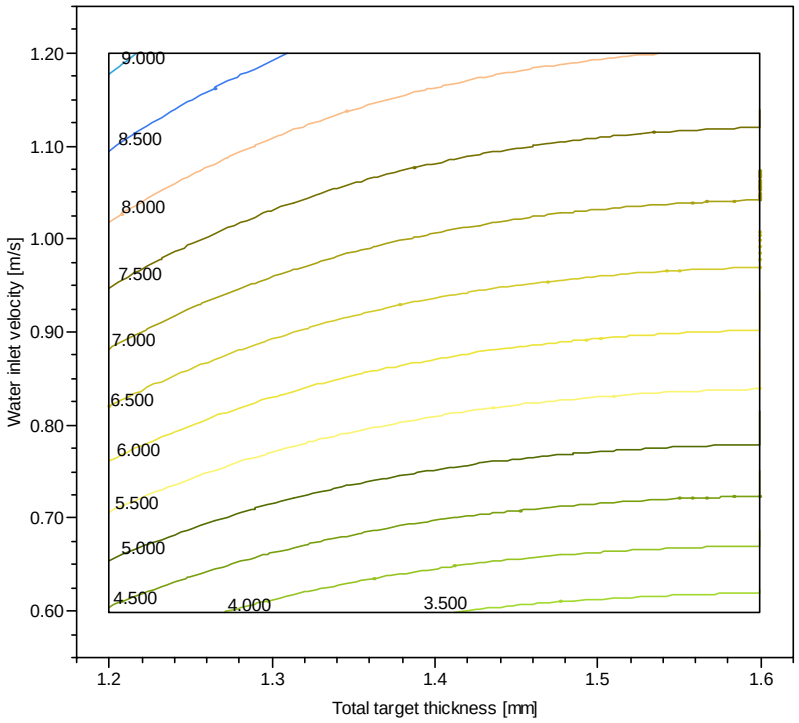

Figure 4.10 – Peak to average ratio contour plot

The peak to average ratio contour plot shows a strong dependence on both total target thickness and water inlet velocity. Constant peak to average ratio lines are developed to provide a straightforward evaluation of the design.

Chapter 5 Conclusions and Future Work

5.1 Conclusions

Computational Fluid Dynamics simulations of a thermal management solution for a wide beam area x-ray source have shown that adequate cooling can be maintained while meeting the design requirements. Three initial target designs been investigated. They have provided valuable information on simulated phenomena and defined the basic principles along which subsequent design development has advanced.

Based on observations and experience accumulated during the development of the initial designs, a final target design has been proposed. A sensitivity study was performed for the final solution by taking into consideration different values for target thickness. Steady state simulations have been performed for both uniform and non-uniform heat flux distributions. The maximum target temperature for a uniform heat flux ($11.693 \cdot 10^6$ W/m^2 / $3.707 \cdot 10^6$ Btu/h·ft^2) considering the maximum target thickness (1.6 mm – 0.063 inch) and the minimum inlet coolant velocity (0.6 m/s – 1.97 ft/s) is 829.22°K (1032.93°F). This value is significantly lower than the melting temperature of the target material, (molybdenum) (2890°K – 4742.33°F). Under these thermal-hydraulic conditions, the minimum water subcooling is 39.12°K (70.37°F), a limit that provides sufficient margin to the onset of boiling. Investigations of the final design performance under non-uniform heat flux

distribution have shown very good operational flexibility. The final design is able to withstand a maximum peak to average ratio of 9.01 for the minimum target thickness (1.2 mm – 0.0472 inch) and the maximum inlet water velocity (1.2 m/s – 3.94 ft/s). This capability is of utmost importance since producing a uniformly distributed heat flux is a challenging task.

The thermal performances mentioned so far are attainable as a result of a water mass flow entering at 293°K (67.73 °F) that continuously removes the heat. The required pumping power is between 84.70 W (0.1137 hp) and 618.99 W (0.8301 hp). Significant reductions in the pumping power are possible if optimized electron distribution on the target is achieved.

5.2 Future Work

Based on the computational studies for the final design, it is important to determine the optimum target thickness and water velocity that provide a balance between the thermal loads under which the target will operate and the costs associated with manufacturing and operation. Additionally, further evaluation of heat dissipated by the target through radiation has to be considered. A suitable management solution should be envisioned such that this concern is properly addressed. Moreover, an external cooling circuit capable of delivering coolant at the required parameters and rejecting the heat load associated with target operation has to be designed. Last, but of equal importance, a good electron distribution and an improved control of electron trajectories which translates in a more uniform heat flux on the target, represents a research focus worthy to be further pursued.

REFERENCES

[1] Anderson, J.D. (1995). “Computational Fluid Dynamics – The Basics with Applications”, McGraw-Hill.

[2] ANSYS Inc. (2006). “ANSYS CFX Introduction”, ANSYS CFX Release 11.0.

[3] ANSYS Inc. (2006). “ANSYS CFX-Solver Theory Guide”, ANSYS CFX Release 11.0.

[4] Ferziger, J.H. and Peric M. (2002). “Computational Methods for Fluid Dynamics”, third edition, Springer.

[5] Versteeg H.K. and Malalasekera W. (1995). “An introduction to computational fluid dynamics - The finite volume method”, Longman Scientific & Technical.

[6] Tennekes, H. and Lumley J.L. (1972). “A First Course in Turbulence”, MIT Press, Cambridge, Massachusetts.

[7] Wilcox D.C. (1994). “Turbulence Modeling for CFD”, DCW Industries, Inc.

[8] Hoffmann K.A. and Chiang S.T. (2000). “Computational Fluid Dynamics – Volume III”, fourth edition, Engineering Education Systems.

[9] Kim, C.H. (2007). “A Study of Monochromatic X-ray Area Beam for Application in Diffraction Enhanced Imaging”, PhD. Thesis, North Carolina State University.

[10] Kim, C.H., Doster J.M. and Bourham M.A. (2009). “Wide-Beam X-Ray Source Target Thermal Management Simulation Using Inner Jet Cooling”, Scholarly Research Exchange, Volume 2009, Article ID 797068.

[11] MatWeb, “100% pure Molybdenum annealed data sheet”, Marketech International Inc.

[12] ANSYS Inc. (2007). “User Manual”, ANSYS ICEM CFD/AI Environment Release 11.0.

[13] Frey P.J. and George P.L. (2000). “Mesh Generation – Application to Finite Elements”, Hermes Science Publishing.

APPENDICES

Appendix A. Non-Uniform Heat Flux Distribution Maps

This section presents selected non-uniform heat flux distribution maps. Figure A.1 shows the heat flux map for the final design version 01, total target thickness 1.2 mm (0.0472 inch), inlet velocity 0.6 m/s (1.97 ft/s) and peak to average ratio 4.37. In Figure A.2 the non-uniform heat flux distribution for the final design version 02, total target thickness 1.4 mm (0.0551 inch), inlet velocity 0.9 m/s (2.95 ft/s) and peak to average ratio 5.79 can be seen. Figure A.3 gives the heat flux map for the final design version 03, total target thickness 1.6 mm (0.063 inch), inlet velocity 1.2 m/s (3.94 ft/s) and peak to average ratio 8.07.

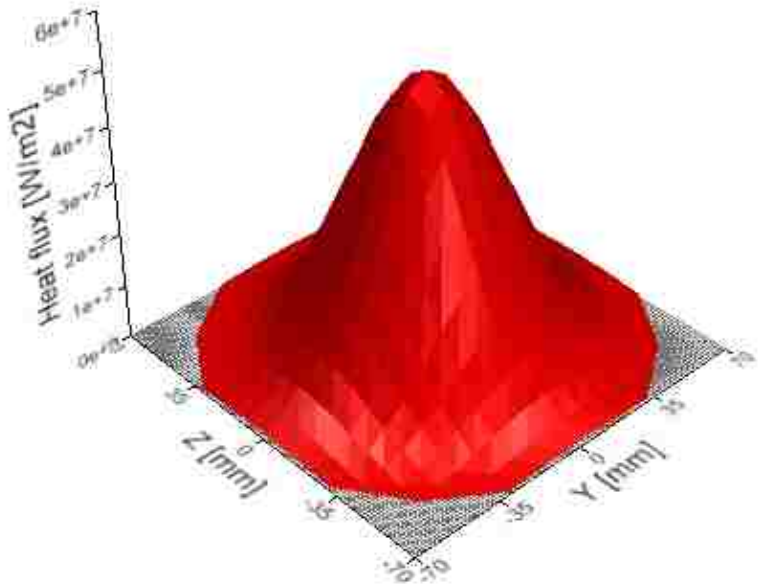

Figure A.1 – Non-uniform heat flux distribution for 4.37 peak to average ratio

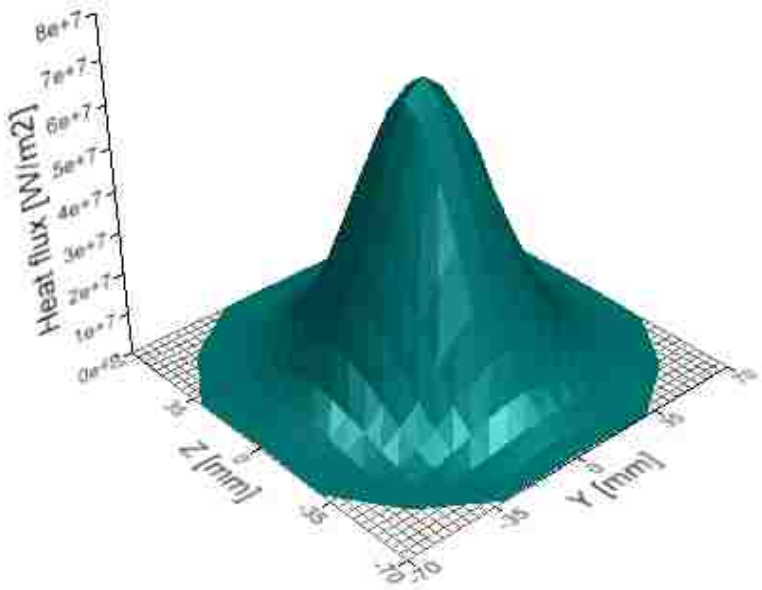

Figure A.2 – Non-uniform heat flux distribution for 5.79 peak to average ratio

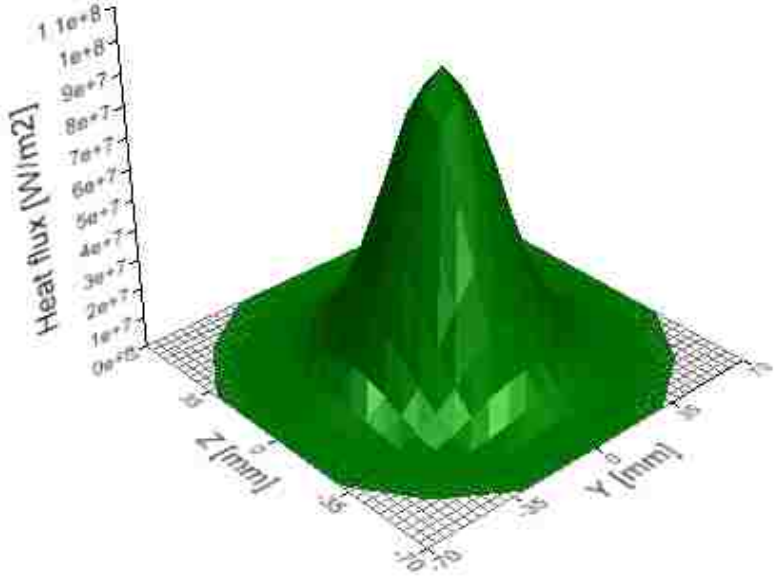

Figure A.3 – Non-uniform heat flux distribution for 8.07 peak to average ratio

Appendix B. ANSYS CFX-Solver Convergence Plots for Uniform Heat Flux Distribution

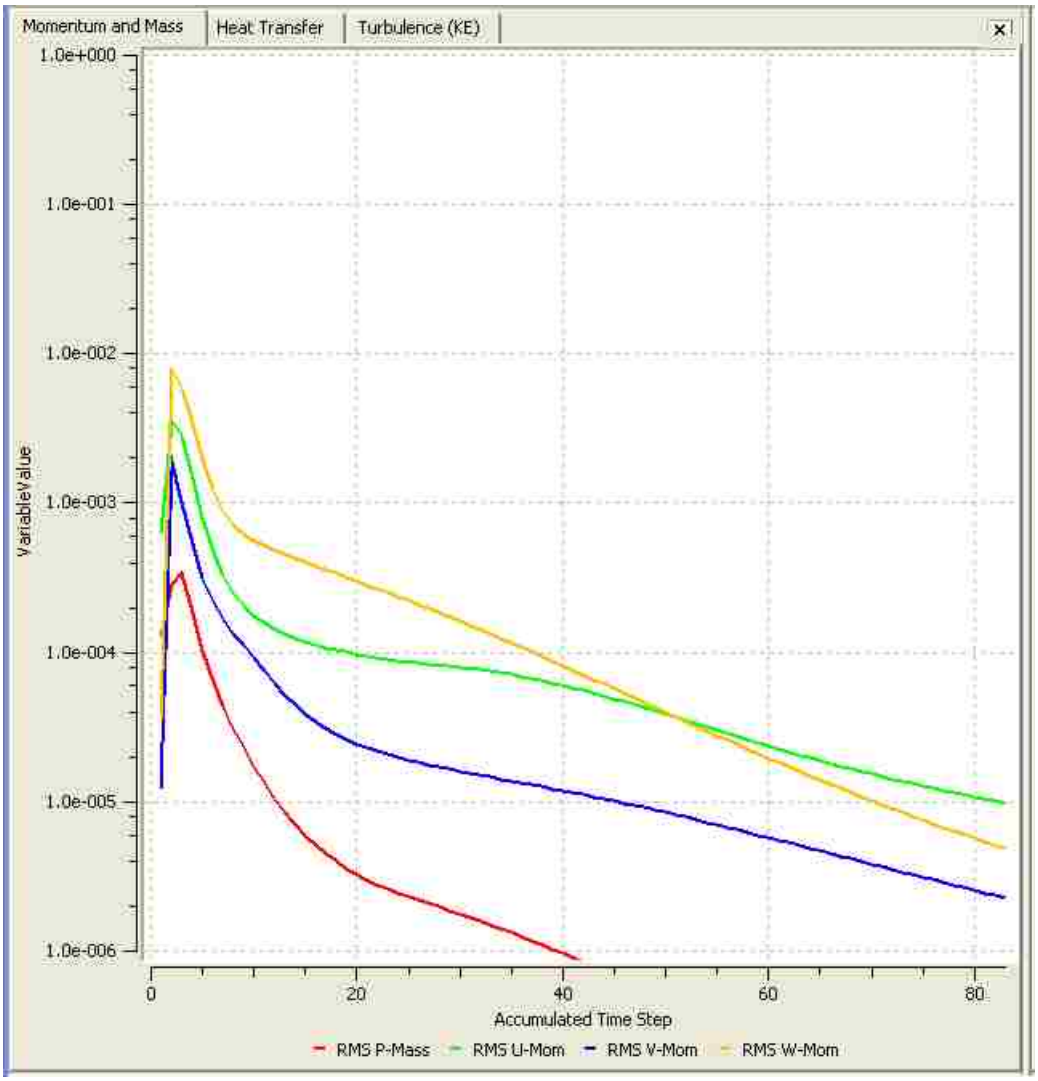

Figure B.1 – Mass and momentum convergence plot for final design ver.01 - 0.6 m/s

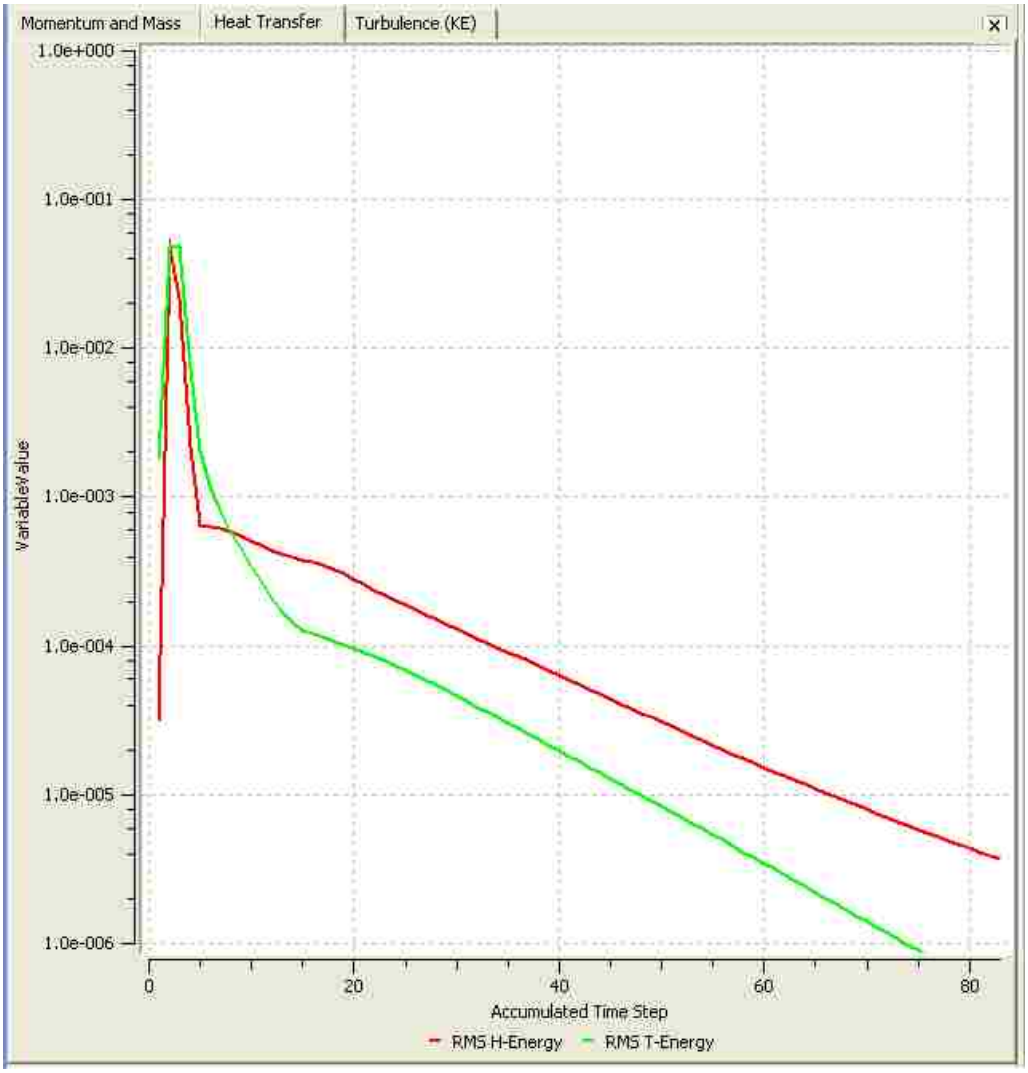

Figure B.2 – Heat transfer convergence plot for final design ver.01 - 0.6 m/s

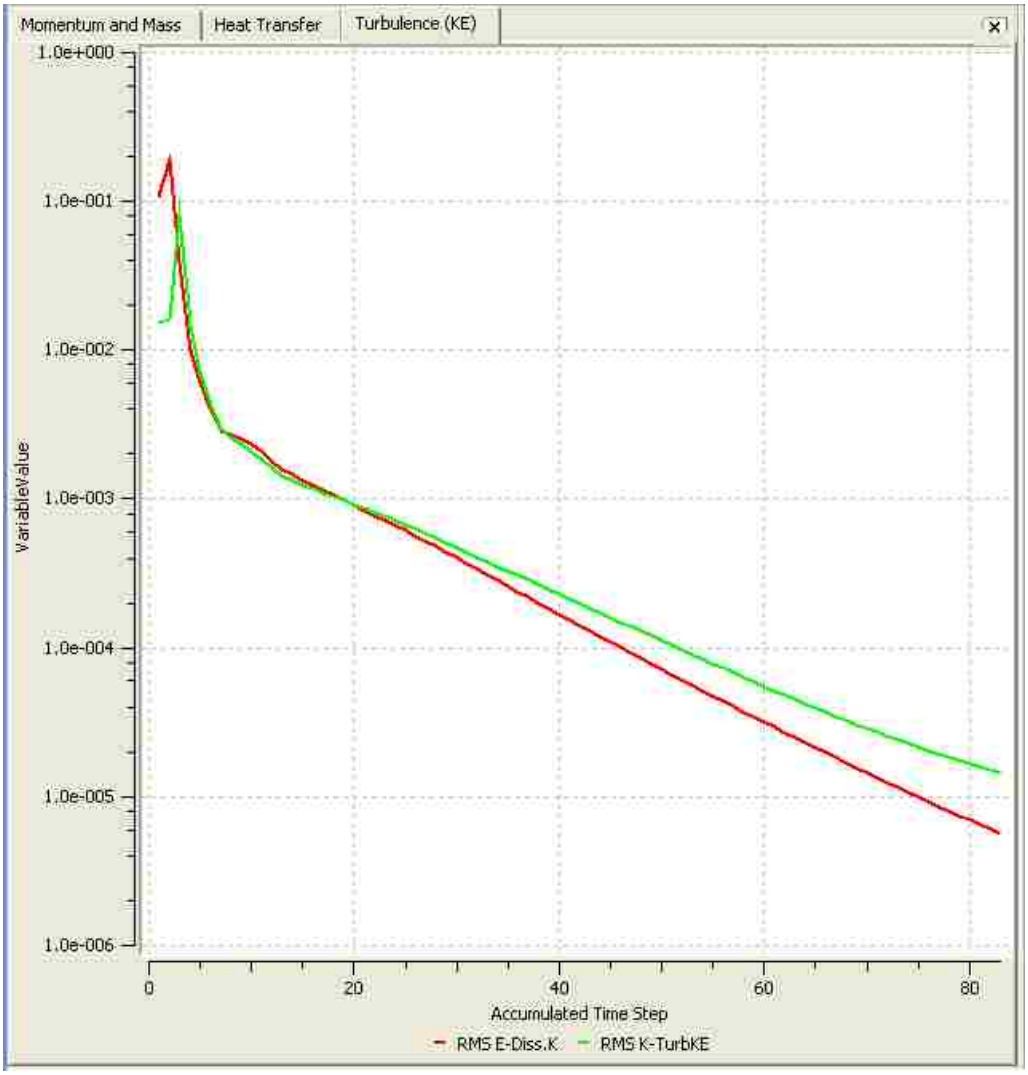

Figure B.3 – Turbulence convergence plot for final design ver.01 - 0.6 m/s

Appendix C. Additional ANSYS CFX Results

This section presents important ANSYS CFX results for final design ver.02 (total target thickness of 1.4 mm – 0.0051 inch) considering a water inlet velocity of 0.9 m/s (2.95 ft/s) for both uniform and non-uniform heat flux distributions. The peak to average ratio for the non-uniform heat flux distribution is 5.79.

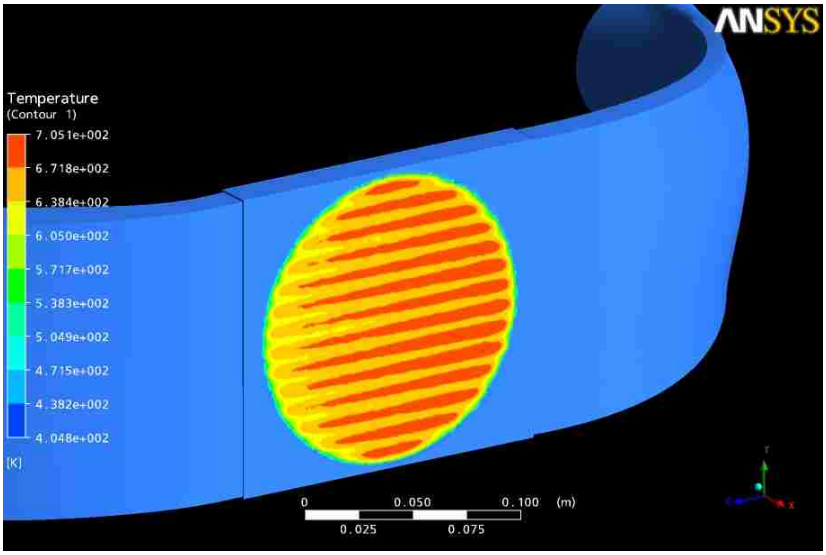

Figure C.1 – Uniform heat flux – Heated target area temperature profile

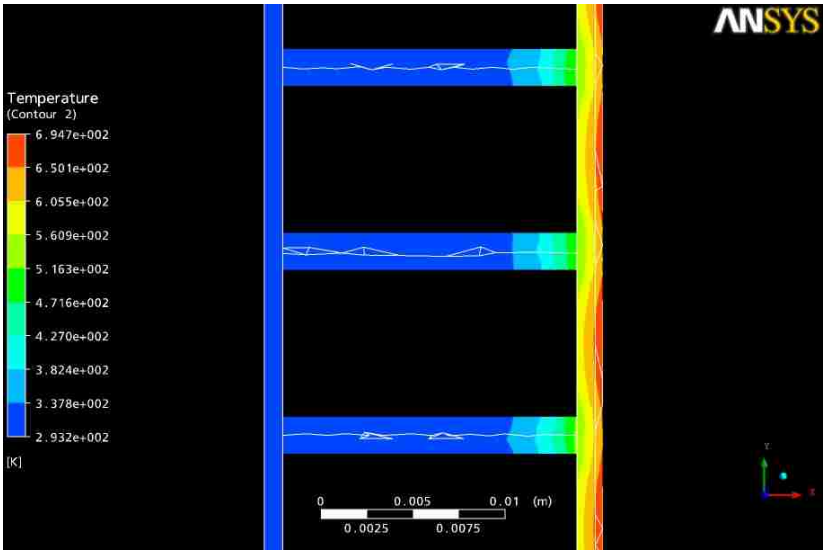

Figure C.2 – Uniform heat flux – Target temperature profile

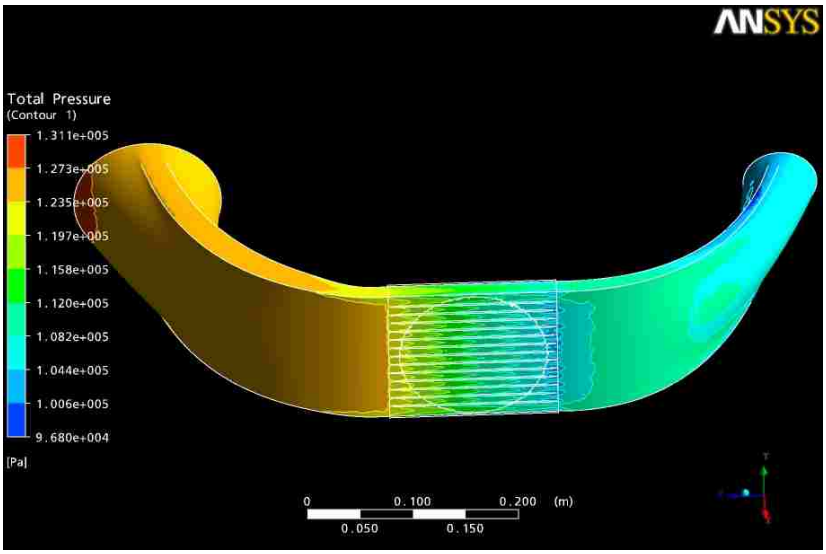

Figure C.3 – Uniform heat flux – Water pressure profile

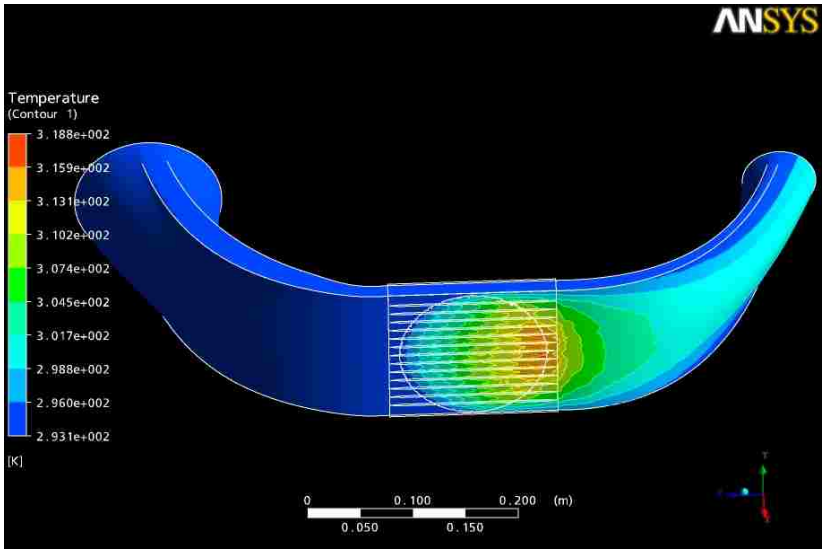

Figure C.4 – Uniform heat flux – Water temperature profile

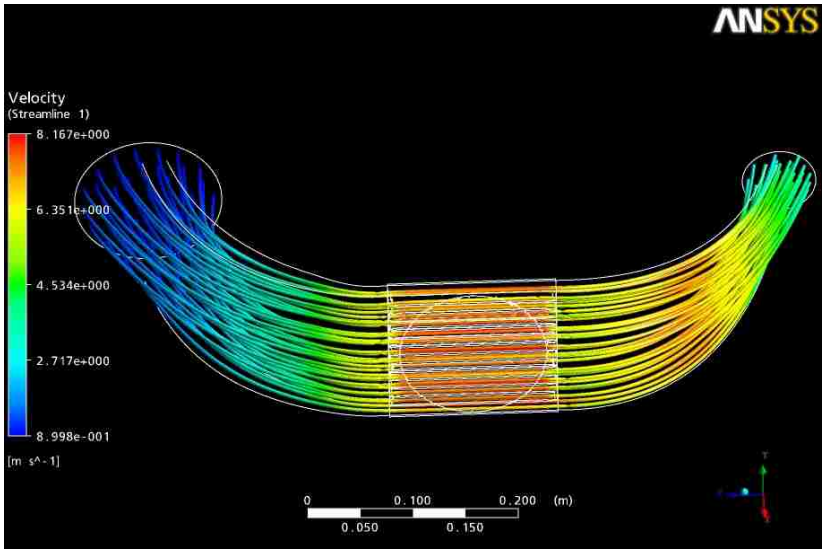

Figure C.5 – Uniform heat flux – Water velocity streamlines

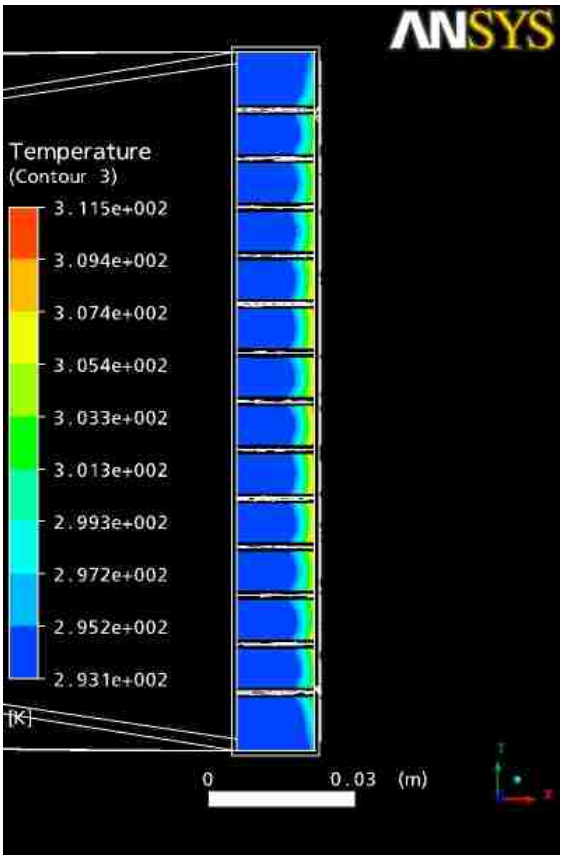

a) Temperature profile

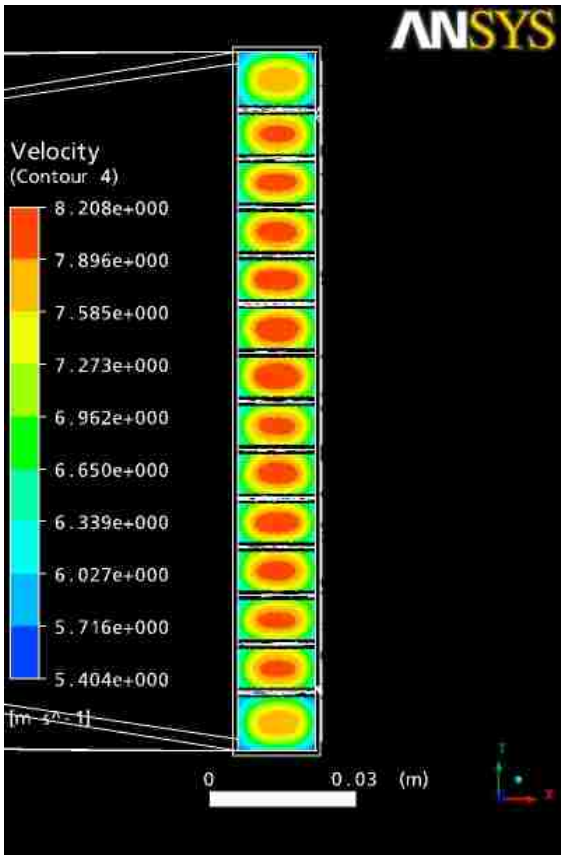

a) Velocity profile

Figure C.6 – Uniform heat flux – Water temperature and water velocity profiles

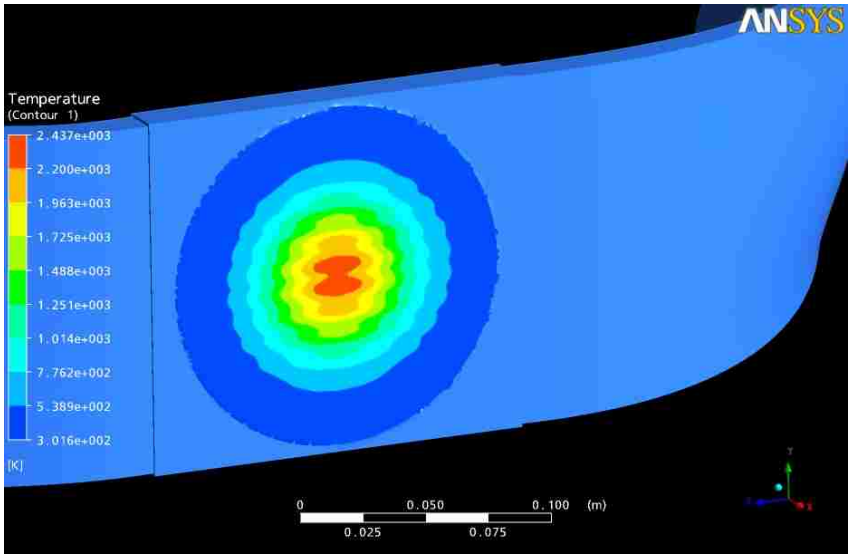

Figure C.7 – Non-uniform heat flux – Heated target area temperature profile

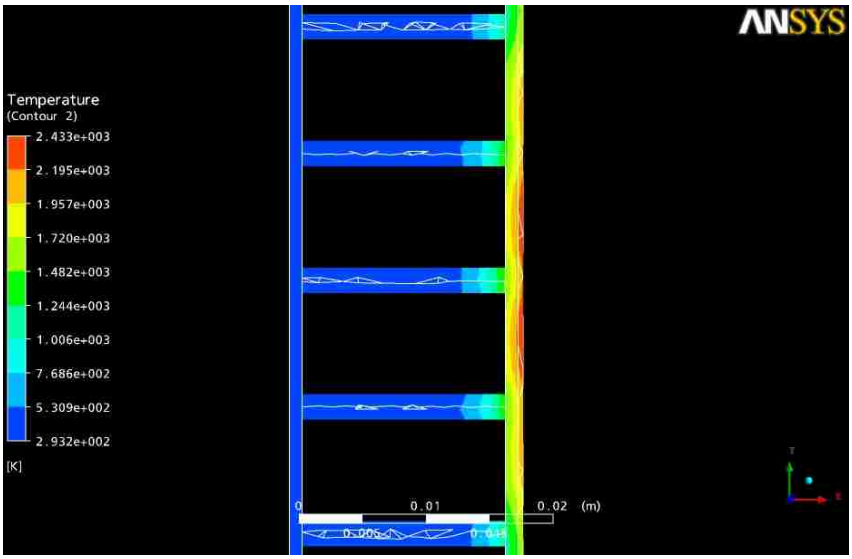

Figure C.8 – Non-uniform heat flux – Target temperature profile

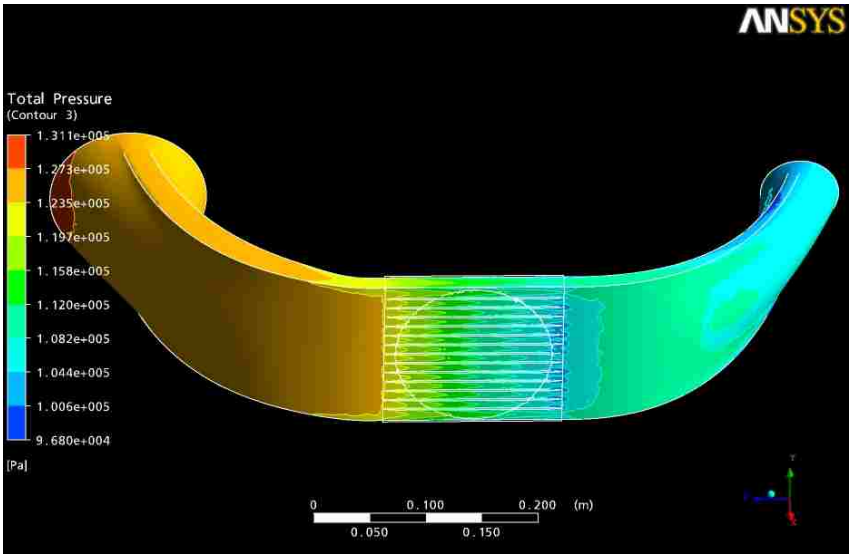

Figure C.9 – Non-uniform heat flux – Water pressure profile

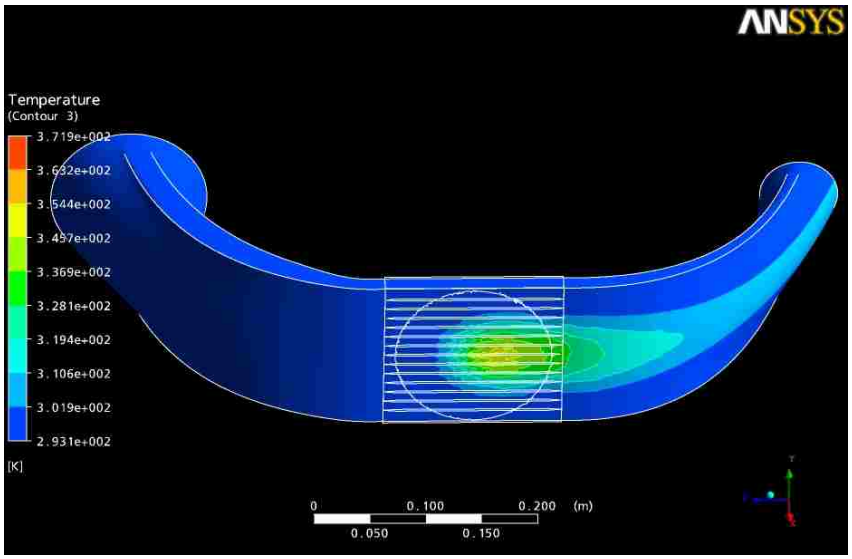

Figure C.10 – Non-uniform heat flux – Water temperature profile

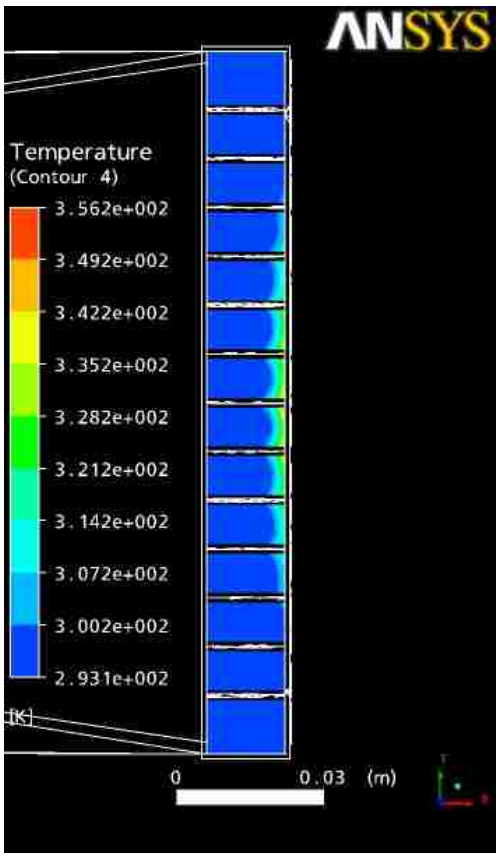

a) Temperature profile

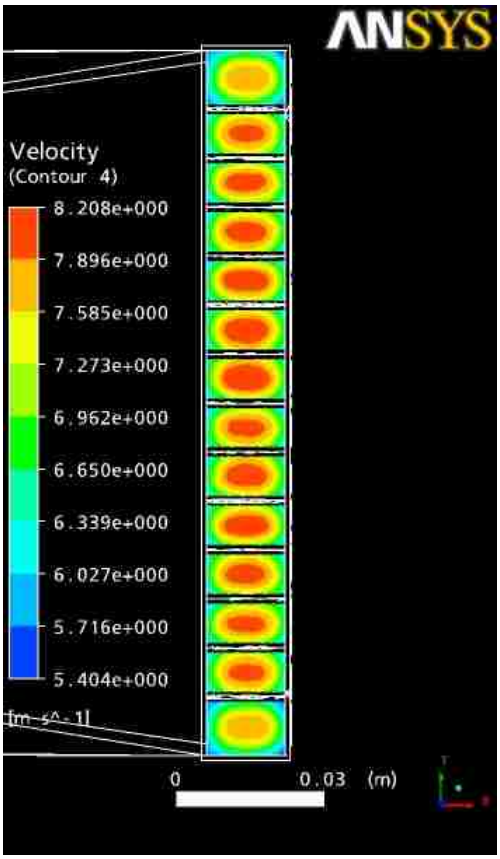

a) Velocity profile

Figure C.11 – Non-uniform heat flux – Water temperature and water velocity profiles